Impact of climate change on the ecology of the Kyambangunguru Crater Marsh in southwestern Tanzania during the Late Holocene

Sarah Coffinet[a][1], Arnaud Huguet[a], Laurent Bergonzini[b], Nikolai Pedentchouk[c], David Williamson[d],

Christelle Anquetil[a], Mariusz Gałka[e], Piotr Kołaczek[e], Monika Karpińska-Kołaczek[e, f, g], Amos

Majule[h], Fatima Laggoun-Défarge[i], Thomas Wagner[j], Sylvie Derenne[a]

[a]*Sorbonne Université, CNRS, EPHE, PSL, UMR METIS, Campus Pierre et Marie Curie, 4 place Jussieu, 75252 Paris cedex 05, France*

[b]*Université Paris Saclay, UPS Univ Paris 11, CNRS, UMR GEOPS, rue du belvédère, Bât 504, 91405 Orsay cedex, France*

[c]*School of Environmental Sciences, University of East Anglia, Norwich Research Park, Norwich, NR4 7TJ, United Kingdom*

[d]*Sorbonne Université, Institut de Recherche pour le Développement, MNHN, CNRS, UMR LOCEAN, Centre IRD France Nord, F-93143, Bondy cedex, France*

[e]*Department of Biogeography and Paleoecology, Faculty of Geographical and Geological Sciences, Adam Mickiewicz University in Poznań, Krygowskiego 10, 61-680 Poznań, Poland*

[f]*Laboratory of Wetland Ecology and Monitoring, Faculty of Geographical and Geological Sciences, Adam Mickiewicz University in Poznań, Krygowskiego 10, 61-680 Poznań, Poland*

[g]*Centre for the Study of Demographic and Economic Structures in Preindustrial Central and Eastern Europe, University of Bialystok, Plac Uniwersytecki 1, 15-420 Białystok, Poland*

[h]*Institute of Resource Assessment, University of Dar Es Salaam, P.O. Box 35097, Dar Es Salaam, Tanzania*

[i]*Université d'Orléans, CNRS, BRGM, UMR ISTO, 1A rue de la Férollerie 45071 Orléans, France*

[j]*Heriot-Watt University, Lyell Centre for Earth and Marine Science and Technology, School of Energy, Geoscience, Infrastructure and Society (EGIS), Edinburgh, EH14 4AS, United Kingdom*

Corresponding author email address: scoffinet@marum.de ; +49 421 218 65740

[1] Present address: Organic Geochemistry Group, MARUM - Center for Marine Environmental Sciences & Department of Geosciences, University of Bremen, Leobener St. 8., Bremen, Germany

32   **Abstract**

33   Instrumental records of temperature and hydrological regimes in East Africa evidence frequent droughts

34   with dramatic effects on population and ecosystems. Sources of these climatic variations remain largely

35   unconstrained, partly because of a paucity of Late Holocene records. Here, we present a multi-proxy

36   analysis of a 4-m continuous sediment core collected in the Kyambangunguru crater marsh, in southwest

37   Tanzania, covering the last 4000 yrs (cal. BP). We used microscopic (macro-remains, microfossils,

38   palynofacies, pollen), elemental (carbon, nitrogen contents), molecular (br GDGTs, n-alkanes) and

39   compound-specific isotopic (δ^2H n-alkanes) investigations to reconstruct the environmental history of

40   the marsh. The multi proxy record reveals that, 2500 years ago, the marsh underwent a major ecological

41   transition from a lake to a peatland. Temperature and hydrological reconstructions evidence warmer and

42   drier conditions between 2200 and 860 cal. BP, which probably triggered the establishment of a

43   perennial peatland. This study is one of the first combined temperature and precipitation record of Late

44   Holocene in the region and highlights changes in the spatial distribution of the East African climate

45   regimes. Several cold periods are observed, between 3300 and 2000 cal. BP and since 630 cal. BP, the

46   latter corresponding to the Little Ice Age. Moreover, wetter conditions are reported during the Medieval

47   Climate Anomaly in contrast to other north-eastern African records suggesting that Tanzania is located

48   at the transition between two hydro-climatic zones (north-eastern versus southern Africa) and has

49   experienced variable contributions of these two zones over the last millennium.

50

54

1. Introduction

Tropical highlands are major sources of food and freshwater for more than 35 tropical countries (Williamson, 2014). The climate dynamics and variability of these topographically complex environments, however, remain poorly studied. While it has been shown that the Quaternary climatic trends in East Africa were primarily controlled by orbital forcing (e.g. Garcin et al., 2006; Tierney et al., 2008), the shorter scale climate dynamics of this region is largely unconstrained. Notably, mid- to late Holocene records of many East African lakes (e.g. Gasse, 2000; Wanner et al., 2011) suggest rapid and frequent, high amplitude, climatic fluctuations at the centennial scale. These fluctuations and their consequences are not well understood due to a general lack of highly resolved records (Nicholson et al., 2013). Furthermore, the timing and intensity of these events are not always synchronous from site to site (Tierney et al., 2011, 2013). Here, we present detailed records of climate and ecosystem changes from a sequence of sediments covering the late Holocene (the last 4000 years) in the Kyambangunguru marsh. This marsh is located in the Rungwe Volcanic Province (RVP; southwest Tanzania), a highland representing one of the four major food crop producing regions in the country (Majule, 2010).

Marshes and peatlands have a great potential for quantitative high-resolution palaeoclimatic records (Amesbury et al., 2012; Blackford, 2000) notably in the tropics (e.g. Bonnefille et al., 1990; Bourdon et al., 2000; Page et al., 2011; Rucina et al., 2010; Swindles et al., 2018). However, they are highly dynamic ecosystems where the vegetation cover and the hydrology functioning can be totally modified at a centennial scale (Loisel and Yu, 2013). This may complicate the interpretation of climatic proxies, notably those based on biological markers as their fluctuations may be related to ecological, local change rather than regional climatic change. A major challenge in using marsh/peat records as climatic archives is thus to disentangle biological signals linked to dynamic changes of the peatland ecosystem itself from those that are driven by local to regional environmental change (Chambers et al., 2012; Morris et al., 2015). The focus of this study is to investigate the internal, ecological changes within the marsh in the context of regional climatic variations. We aim to retrieve detailed (quantitative) air temperature and (qualitative) hydrological condition records of the late Holocene from the southernmost part of East Africa to test whether rapid and high amplitude climatic events (e.g. Russell and Johnson, 2005; Wanner

82 et al., 2011) were recorded in this area in comparison to other East African records. Additionally, the

83 multi-proxy approach, combining microscopic observations and geochemical characterization, intends

84 to determine potential feedbacks of these rapid climatic events in the tropical highland wetlands as well

85 as potential human impact in the region.

86 Analysis of pollen, non-pollen palynomorphs (NPPs), macro-remains, palynofacies and bulk elemental

87 (C and N content) determination was conducted to characterize the ecological states of the wetland,

88 complemented by biomarker-based proxies to determine past variations in air temperature and

89 hydrology. Branched glycerol dialkyl glycerol tetraethers (br GDGTs) and compound specific long

90 chain n-alkane hydrogen isotopic composition (δ^2H_{wax}) were used for mean annual air temperature and

91 hydrological conditions reconstruction, respectively. Br GDGTs are membrane lipids produced by

92 unknown bacteria (Sinninghe Damsté et al., 2000) whose relative abundances in environmental samples

93 have been shown to correlate with temperature and pH (Weijers et al., 2006, 2009). This enabled the

94 reconstruction of past pH and air temperatures from the br GDGT distribution in sediments, peats and

95 soils (Nichols et al., 2014; Peterse et al., 2011; Weijers et al., 2007a). Long chain n-alkanes are

96 constituents of the epicuticular wax layer of leaves (Eglinton and Hamilton, 1967). It has been shown

97 that their hydrogen isotopic composition (δ^2H_{wax}) reflects the hydrogen isotopic composition of the water

98 taken up by the plants (e.g. Estep and Hoering, 1980; Sauer et al., 2001; Sessions et al., 1999).

99 Accordingly, they can be used to reconstruct variations in local palaeohydrology as shown in several

100 lacustrine sedimentary archives from the Quaternary and the Holocene in East Africa (e.g. Loomis et

101 al., 2015; Powers et al., 2005; Tierney et al., 2008; Verschuren et al., 2000). The combined use of these

102 two proxies allows distinguishing the temperature from the hydrological signal which has been a major

103 limitation in lake-based East African climatic reconstructions (Verschuren, 2003). Moreover, in settings

104 with high sedimentation rates like marshes, they can offer highly detailed and independent

105 reconstruction of the temperature and the hydrological conditions.

106

107

108

2. Regional setting: the Rungwe Volcanic Province and the Kyambangunguru marsh

The Rungwe Volcanic Province (RVP; SW Tanzania; Fig. 1A), is a large volcanic mountain region (1500 km²) located at the triple junction of the Malawi Rift, Rukwa/Tanganyika Rift and the Usanga Basin in the southern part of the East African Rift System (Fontijn et al., 2010, 2012). The RVP is delimited by the Poroto Mountains in the north, Lake Malawi in the south and the Livingstone escarpment in the west (Fig. 1B). The area is known to be seismically active with volcanic eruptions occurring from the late Miocene (9.2 Ma) to the 19th century, with hot spring activity still found today (Branchu et al., 2005). The region contains three major stratovolcanoes: the Ngozi, Kyejo and Rungwe (Fontijn et al., 2010, 2012). South of these high-altitude sites and north of Lake Malawi lies the Karonga plain. Several monogenic maar-type craters were created during late Pleistocene phreatomagmatic explosions along the Mbaka fault system and are now filled by closed lake hydro-systems (Fontijn et al., 2012; Fig. 1B). The region belongs to the humid equatorial zone of Africa, mainly determined by the migration of the Intertropical Convergence Zone (ITCZ), a key atmospheric feature of tropical atmospheric circulation with low-pressure air masses accompanied by high precipitation. The ITCZ reaches its southernmost position (centred at ca. 15°S, Fig. 1A) in January, resulting in seasonal fluctuations between hot humid conditions from November to May and relatively colder and dry conditions from June to October (Fig. 1C). The RVP is among the most humid regions of Tanzania along with the coastal zone (Basalirwa et al., 1999). It is characterized by a different rainfall distribution with persisting rainfall in April-May. Nivet et al. (2018) showed that the Indian tropical Ocean and the Austral Ocean are the main sources of moisture in the area, with only a minor influence of the Congo Air Mass. Thus, the currently observed variability of the regional rainfall is likely highly impacted by the Indian Ocean Dipole, through Sea Surface Temperature anomalies. Over the last century, climatic trends from the RVP point towards drier conditions associated with a shorter rain season (Williamson et al., 2014) and a continuous increase in temperature ($\approx$ 1°C for the last 100 yr.; Branchu et al., 2005). Typical vegetation of the region includes Zambezian Miombo-type woodland at low altitude and Afromontane vegetation at higher altitude (Garcin et al., 2006, Williamson et al., 2014). In many locations, the woodland has been replaced by diverse crops (banana, rice, cocoa, tea, coffee, maize;

136   Coffinet et al., 2017; Williamson et al., 2014). The RVP is today one of the main agricultural resources

137   of Tanzania (Majule, 2010).

138   The Kyambangunguru marsh (9°22' S - 33°47' E, 660 m a.s.l.) is located in one of the numerous maar

139   craters of the RVP, between the Mbaka River and the Mbaka fault. These maar craters are essential

140   water and biodiversity resources for the region. At Kyambangunguru, no human activity has been

141   recorded nor is known within the crater (no land or water use). Human settlement expands in the plains

142   surrounding the volcano (mainly family-scale farming) but not on its slopes. The inner marsh covers

143   about 0.04 km² and its catchment area – limited to the crater slopes elevated ca. 100 m above the water

144   table – is relatively small (0.20 km²; Delalande et al., 2008a, Fig. 1D). According to the Lwifwa Masoko

145   station of the University of Dar es Salaam located at Lake Masoko, 7.5 km to the south east, mean

146   precipitation (P) is up to 2099 mm.yr^{-1}, with April being the most humid month (470 mm in average)

147   and September the driest one (8 mm in average; Nivet et al., 2018). Air temperature fluctuates around

148   22 °C throughout the year; July is the coldest month (19 °C on average) and November the warmest (25

149   °C on average). The crater depression is filled with peat like deposits overgrown by marsh-type

150   vegetation and the water level (H) varies around 70 cm of amplitude over the year (Fig. 1C). At the end

151   of the rainy season, the marsh resembles a shallow lake with floating vegetation mats and patches of

152   free water surface (Fig. 1E) while the water table considerably decreases during the dry season (Fig.

153   1C). On a monthly scale, water level fluctuations (ΔH) correlate with the rainfall (P): ΔH = 1.03 P – 18

154   (in cm; n = 12; r = 0.97). During the humid season, the marsh water is warm (around 25 °C), low

155   mineralized and slightly acidic (pH around 5.8). On the contrary, during the dry periods, it is

156   characterized by higher mineral concentration as well as pH increase up to around 6.4, because of water

157   evaporation at the surface (Delalande, 2008; Delalande et al., 2008a). The water residence time in the

158   marsh is short (a few months), based on the isotopic water budget of the marsh in- and outputs (δ^{18}O

159   and δ^2H of H_2O; Delalande et al., 2008a), suggesting a prominent influence of climate in the marsh

160   water budget. The isotopic signature of the marsh water during the humid season (δ^2H-H_2O = -7‰) is

161   close to the mean annual isotopic signature of precipitation recorded at Lwifwa Masoko station (Nivet

162   et al., 2018). At the end of the dry season, the marsh water isotopic signature (δ^2H-H_2O) becomes more

163   ^{2}H-enriched (between 7 and 16‰, Fig. 1C) demonstrating significant evaporation resulting from the

164 drier climatic conditions. The slopes of the crater are steep and covered by Zambezian-type (Miombo)

165 forest, dominated by *Brachystegia*, *Uapaca* and *Acalypha* tree species, all common to the region (White,

166 1983). Shrubs of Rubiaceae and Myriaceae families are present at the edge of the marsh. The vegetation

167 of the marsh is dominated by sedges (*Carex, Cyperus*) while floating (*Nymphaea*) and submerged

168 macrophytes are abundant in the depressions filled with water during the rainy season.

169

170 **3.   Materials and methods**

171   3.1. Core retrieval and sampling

172 A 4-m long core was collected with a Wright corer in the Kyambangunguru marsh in December 2012.

173 The coring process was stopped at 4 m because of the thickness of the Rungwe Pumice tephra (Fontijn

174 et al., 2012) and thus covers the most recent history of the Kyambangunguru wetland. The core was

175 sampled in 1 cm thick slices at the Lwifwa-Masoko station of University of Dar es Salaam and kept at

176 -20 °C until further treatment. 21 samples were chosen for dating while 35 samples were selected every

177 12 cm to perform the elemental (carbon and nitrogen content), molecular (br GDGTs, *n*-alkanes) and

178 isotopic (δ^2H_{wax}) analyses. Total organic carbon (C_{org}) and nitrogen (N) contents were determined after

179 decarbonatation by elemental analysis at the Service Central d'Analyse du CNRS, Villeurbanne, France.

180 105 1 cm-thick samples (ca. every 3 cm) were selected for plant macrofossil analysis. Among these, 44

181 samples (distributed evenly along the core) were additionally analysed for pollen and non-pollen

182 palynomorphs (NPPs). Within these 44 samples, 12 were used for palynofacies determination.

183 Additionally, 5 surface soil samples (0-5 cm) from the catchment area were collected between the marsh

184 and the top of the crater.

185

186   3.2. Absolute chronology and sediment accumulation rate

187

188 The chronology of the core is based on 21 Accelerator Mass Spectrometry (AMS) dates performed on

189 bulk Total Organic Matter (TOM; 17 samples) and wood fragments (4 samples; Table 1) all along the

190 core. Samples were subjected to acid-alkali-acid treatment to remove the mineral phase. AMS-^{14}C and

191 associated $\delta^{13}C$ analyses were conducted on aliquots prepared according to the following AMS protocol:

192 burning at 860 °C for 30 min under vacuum, in the presence of a Cu (II)-oxide/Cu (III)-oxide mix and

193 of Ag string. The obtained CO_2 was graphitized on powdered Fe with H_2 at 650 °C for 100 min, and

194 graphite was compressed in analytical pellets. Residual CO_2 gases were used for associated ^{13}C

195 measurements on a SIRA 10 and are expressed in delta notation per mil versus V-PDB (Vienna Pee Dee

196 Belemnite). Graphite preparation and $\delta^{13}C$ measurements were made at the GEOPS Laboratory

197 (University of Paris-Saclay, France). ^{14}C counting was performed using the AMS facility at the LMC14

198 laboratory (Laboratoire de Mesure du Carbone 14; Artemis, Saclay; Cottereau et al., 2007). Analytical

199 uncertainties, are $\pm 0.1‰$ for $\delta^{13}C$ and between 0.2 and 0.5 pMC (percentage of Modern Carbon) for ^{14}C

200 activity.

201 Calibrated radiocarbon ranges were obtained using OxCal 4.3 software (Bronk Ramsey, 2009) with the

202 ShCal13 (Hogg et al., 2013) and Bomb13SH3 (Hua et al., 2013) atmospheric curves as the calibration

203 set (Table 1). A Bayesian age-depth model was used to establish an absolute chronology based on these

204 calibrated ^{14}C date ranges. The age-depth model was constructed applying a *P_Sequence* function, with

205 the parameters $k_0=1$ and $log_{10}(k/k_0)=1$, in the OxCal v. 4.3 software (Bronk Ramsey, 1995, 2008).

206 Additionally, boundaries reflecting potential changes in the rate of deposit accumulation were

207 introduced to the model, based on observations of micro- and macrofossils (see section 4.5 and 4.6).

208 These boundaries were defined as follows: (i) 417.5 cm: top of the tephra layer and bottom of the model,

209 (ii) 191 cm: abrupt change from lacustrine to marshland conditions, (iii) 115.5 cm: distinct increase in

210 water table and (iv) 0 cm: top of the core. Computing of the age-depth model led to the exclusion of two

211 samples (SacA40028 and SacA38523). Dates with the lowest individual agreement between the

212 modelled and the calibrated date, i.e. SacA40077 and SacA40076, were also excluded from the

213 calculations until the lowest critical value of the agreement index (A_{model}) suggested by Bronk Ramsey

214 (2008) for model reliability ($A_{model} = 60\%$) was achieved. Final A_{model} value of the chronology was 63%.

215 The age is presented as a μ (mean) value of the modelled age expressed as calibrated year before present

216 i.e. AD 1950 (cal. BP; Fig. 2), rounded to tens.

217 A mean value for the sedimentation accumulation rate (SAR), expressed in cm year^{-1}, was determined

218 as the median value of the probability distribution of the modelled age (μ) for each depth (in cm) at

219 which a date was modelled. The applied formula was the following:

220 $$\text{SAR} = \frac{1}{\mu_{depth-0.5} - \mu_{depth+0.5}} \qquad (1)$$

221

222 ### 3.3. Plant macrofossil analysis

223 About 5 cm^3 of sediment were rinsed with warm water and sieved at 0.25 mm. Macrofossils were studied

224 in transmitted light with a Nikon SMZ800 stereoscopic microscope at a magnification of 10 to 200.

225 Species determination of individual plant macrofossils was performed based on the data from

226 Velichkevich and Zastawniak (2006, 2009). The data were presented as numbers of detected

227 macrofossils and were presented as diagram drawn in the POLPAL software (Nalepka and Walanus,

228 2003). Analysis was performed at the Adam Mickiewicz University in Poznań (Poland).

229

230 ### 3.4. Pollen, non-pollen palynomorphs and microscopic charcoal

231 Samples for pollen, non-pollen palynomorph and charcoal analysis were prepared using standard

232 laboratory procedures: adding 10% HCl to dissolve carbonates, heating in 10% KOH to remove the

233 humic fraction and at least 24-hour treatment with HF to remove the mineral fraction followed by

234 acetolysis (Berglund and Ralska-Jasiewiczowa, 1986). *Lycopodium* tablet of known number of spores

235 (n=20848, produced by Lund University) was added to each sample for calculation of microfossil

236 concentration (Stockmarr, 1971). Pollen and spores were counted with a biological microscope under

237 400× and 1000× magnification until the number of at least 500 pollen grains was obtained (Vincens et

238 al., 2003, 2007). Pollen grains were identified using atlases (Gosling et al., 2013), internet-based

239 databases such as African Pollen Database (http://apd.sedoo.fr/), and the Universal Pollen Collection

240 (Institut des Sciences de l'Évolution Montpellier; http://www.palyno.org/). Non-pollen palynomorphs

241 (NPPs) were identified using available literature (Gelorini et al., 2011; Miola, 2012; van Geel et al.,

242   2011). The NPP type numbers follow the convention of 'HdV-number' and 'UG-number', in which

243   acronym 'HdV' means Hugo de Vries Laboratory of the University of Amsterdam (The Netherlands),

244   whereas 'UG' is Universiteit Gent (Belgium) (Miola, 2012). Percentages of pollen grains originating

245   from forest and savannah communities were calculated as the ratio of an individual taxon and the TPS

246   (total pollen sum); the TPS consists of the sum of AP (arboreal pollen) and NAP (non-arboreal pollen

247   but excludes any taxa originating from aquatic and wetland plants as well as spores and NPPs).

248   Percentages of aquatic and wetland pollen taxa, as well as spores and NPPs, were calculated as the ratio

249   of an individual taxon or NPP type and the TPS enlarged by this taxon or NPP type.

250   Microscopic charcoal particles (size range 0.02-0.5 mm) were counted on the same microscopic slides

251   as the ones used for pollen counting until the total number of charcoal particles and *Lycopodium* spore

252   standard was at least 200 in each sample (Finsinger and Tinner, 2005). Values are expressed as the

253   charcoal accumulation rate (CHARmicro) in grains cm^{-2} $year^{-1}$ and were calculated based on the

254   following formula proposed by Davis and Deevey Jr.(1964):

$$CHAR_{micro} = CHAC_{micro} \times SAR \quad (2)$$

256   where $CHAC_{micro}$ is the concentration of microscopic charcoal particles (in grains or particles cm^{-3}) and

257   SAR is the sediment accumulation rate (in cm $year^{-1}$). The diagrams were prepared using the POLPAL

258   software (Nalepka and Walanus, 2003) and the analyses were performed at the Adam Mickiewicz

259   University in Poznań (Poland).

260

261   3.5. Quantitative palynofacies analysis

262   Sample preparation included treatment with 50 ml of HF overnight at 40°C followed by 50 ml of HCl

263   for 30 min to eliminate siliciclastic and carbonate minerals. Samples were then rinsed until neutral pH.

264   Quantification of the different types of organic matter (OM) is based on the methodology developed by

265   Graz et al. (2010) using incorporation of a standard solution of *Cupressus* pollen at 10 mg.ml^{-1} in each

266   sample. Samples were prepared in thin sections before optical investigations using a transmitted light

267   microscope with a 50× magnification. Particle identification was performed using the methodology

268 described by Boussafir et al. (2012) and Graz et al. (2010). Particles were classified into 3 types: (i)

269 Ligno-Cellulosic tissues (LC) at different stages of degradation comprising fresh tissues detected as

270 translucent LC (tLC), slightly degraded/amorphised LC (saLC) with cell structures that are still partially

271 recognizable and totally degraded/amorphous LC, characterised by red aggregates of amorphous OM

272 (rAOM) as originally described by Graz et al. (2010), (ii) mycelium fragments (myc; Graz et al., 2010)

273 and (iii) planktonic remains (algal organic matter, algOM; Boussafir et al., 2012). Whenever necessary,

274 particle identification was aided using UV excitation. The total mass of each particle type was

275 determined after 40 counting according to Eq. 3:

276 $$m_{part} = \frac{m_{std} \times A_{part}}{A_{std}} \times \frac{d_{part}}{d_{std}} \qquad (3)$$

277 with m_{part}: mass of the particle; m_{std}: mass of the standard; A_{part}: counted surface of the particle; A_{std}:

278 counted surface of the standard; d_{part}: density of the particle; d_{std}: density of the standard. Densities used

279 for the calculation were determined by Graz et al. (2010). Results are expressed as relative abundance

280 (in terms of mass) of each particle to the total. Sample preparation and analysis were performed at the

281 University of Orléans (France).

282

283   3.6. Biomarker analyses

284   *3.6.1. Lipid extraction*

285 After freeze-drying, samples were submitted to a modified Bligh-Dyer extraction as described in

286 Coffinet et al. (2015). The total lipid extract was then separated into three fractions on a silica column

287 with a succession of (i) DCM, (ii) DCM:acetone (2:1, v:v) and (iii) DCM:MeOH (1:1, v:v) followed by

288 pure MeOH as solvents (Coffinet et al., 2015). The apolar fraction containing the *n*-alkanes and the

289 intermediate polarity one (fraction 2) containing the GDGTs were analysed. Prior to analysis, the apolar

290 fraction was further separated on silver nitrate impregnated silica columns (10%, w:w) in Pasteur

291 pipettes (with heptane and then DCM as eluents) in order to purify the linear *n*-alkanes for compound-

292 specific δ²H analysis.

293   *3.6.2. n-Alkane analyses*

294   *n*-Alkanes were analysed at Sorbonne University (Paris, France) by gas chromatography coupled to a

295   mass spectrometer (GC-MS) using an Agilent Network 6890 GC System coupled with a 5973 Mass

296   Selective Detector, with electron impact at 70 eV. 1 µl was injected and separation was achieved using

297   a Restek RXI-5 Sil MS silica capillary column (30 m × 0.25 mm i.d., 0.50 µm film thickness) with He

298   as the carrier gas at 1 ml min^{-1} flow rate. Initial temperature was set at 50 °C and increased to 320 °C at

299   4 °C min^{-1}. Samples were injected in splitless mode and the injector temperature was 280 °C.

300   The average chain length (ACL; Eq. 4) describes the *n*-alkane distribution profile of a sample and is

301   used to determine the predominant origin of the *n*-alkanes. Typically, *n*-alkanes with chain with less

302   than 21 carbon atoms are suggested to be produced by algae and cyanobacteria (e.g. Han et al., 1968)

303   while *n*-alkanes with more than 25 carbon atoms more likely originate from terrestrial higher plants

304   (Eglinton and Hamilton, 1967). *n*-Alkanes with chain length between 21 and 25 carbon atoms are

305   predominantly found in aquatic macrophytes (Ficken et al., 2000).

306    $$\text{ACL} = \frac{\sum C_i \times i}{\sum C_i} \qquad \text{where } i \text{ spans from 21 to 35} \qquad (4)$$

307   The carbon preference index (CPI; Eq. 5) is a ratio assessing the relative importance of odd over even

308   homologues and reflects the degree of maturity (organic matter degradation) of a sample. Immature

309   samples have very high CPI (>> 1; Killops and Killops, 2005). Unusually low CPI (below 3) in recent

310   sediments are generally considered as polluted by a source of mature organic matter (petroleum, wood

311   burning; Bray and Evans, 1961).

312    $$CPI = 0.5 \times \left(\frac{\sum C_{odd\,25-33}}{\sum C_{even\,24-32}} + \frac{\sum C_{odd\,25-33}}{\sum C_{even\,26-34}} \right) \qquad (5)$$

313   The P_{aq} index (Eq. 6) was developed by Ficken et al. (2000) and is a proxy for the relative contribution

314   of emergent/terrestrial macrophytes compared to submerged/floating ones. Contribution of submerged

315   and floating macrophytes is considered as high when P_{aq} values are higher than 0.4 and insignificant

316   when P_{aq} values are lower than 0.1.

317    $$P_{aq} = \frac{C_{23} + C_{25}}{C_{23} + C_{25} + C_{29} + C_{31}} \qquad (6)$$

318   *n*-Alkane hydrogen isotopic composition (δ^2H *n*-alkane) was measured at Newcastle University (United-

319   Kingdom) using a Delta V+ isotope-ratio mass spectrometer (IRMS, Thermo Fisher) connected to a GC

320   Ultra Trace (Thermo Fisher), a Finnigan GC Combustion III (Thermo Fisher) and a high temperature

321   conversion (HTC) system set up at 1400 °C. The GC temperature was set to start at 50 °C and then to

322   raise to 250 °C at 15 °C min^{-1} and from 250 °C to 320 °C at 5°C min^{-1}. Temperature was then held at

323   320 °C for 15 min. Every sample was analysed in duplicate and the ^{2}H/^{1}H ratio was reported on the V-

324   SMOW (Vienna standard mean ocean water) scale and expressed in delta per mil (δ‰). A mixture of

325   *n*-C$_{16}$ to *n*-C$_{30}$ alkane standard and 5α androstane standard (A. Schimmelmann, Indiana University) was

326   run at the beginning and at the end of each sequence. Standard error of the measurements of the

327   individual long chain *n*-alkanes (C$_{23}$-C$_{31}$) from this standard mix ranged between 0.3‰ and 1.1‰.

328   *3.6.3. GDGT analysis*

329   GDGTs were analysed at Sorbonne University (Paris, France) with a high-pressure liquid

330   chromatography coupled to a mass spectrometer with an atmospheric pressure chemical ionization

331   source (HPLC-APCI-MS, Shimadzu LCMS-2020). Separation was achieved with a Prevail Cyano

332   column (2.1 mm x 150 mm, 3 µm; Alltech, Deerfield, IL, USA) at 30 °C, using a mixture of hexane and

333   isopropanol at 0.2 ml min^{-1} according to Coffinet et al. (2015). Elution began at 99% A/1% B for 5 min

334   followed by a linear gradient to 98% A/2% B in 45 min. A second linear gradient led to a mixture of

335   90% A/10% B in 10 min, maintained for 10 min and returned to the initial conditions (99% A/1% B) in

336   14 min, maintained for 10 min. Injection volume was 10 µl. Single ion monitoring (SIM) of the [M+H]$^+$

337   ions was used to detect the GDGTs.

338   Mean annual air temperatures (MAAT) were estimated using the calibration specifically developed for

339   East African lakes by Loomis et al. (2012):

340    $$MAAT = 22.77 - 33.58 \times f(III) - 12.88 \times f(II) - 418.53 \times f(IIc) + 86.43 \times f(Ib) \qquad (7)$$

341   where f(x) is the fractional abundance of the compound x relative to the total br GDGTs and the roman

342   numerals correspond to the different br GDGT compounds according to Weijers et al. (2007b)

343   numbering.

344 pH was calculated using the soil calibrations developed by Tierney et al. (2010b) and based on the

345 cyclisation ratio of br GDGTs (CBT; Weijers et al., 2007b):

346 $$pH = 10.32 - 3.03 \times CBT \qquad (8)$$

347 $$CBT = -\log\left(\frac{[Ib] + [IIb]}{[I] + [II]}\right) \qquad (9)$$

348 where the roman numerals correspond to the different br GDGT compounds according to Weijers et al.

349 (2007b) numbering.

350

351 **4.   Results**

352   4.1. Lithology

353 The bottom of the core corresponds to a pumice-rich tephra. The overlaying deposits (ca. 418 to 200

354 cm) consist of an alternating layer of peat, organic gyttja and silty clay material, with charcoal-rich

355 layers (Fig. 2). Above 200 cm, the sediment mostly consists of peat at diverse stages of decay. Large

356 amounts of higher plant macrofossils are observed at depth ranging between 175 and 75 cm, while the

357 decomposition of plant fragments is more pronounced from 75 cm to the top of the sequence. The upper

358 clayey part of the sequence contains two additional tephra layers at 65.5-63 cm and at 57-51 cm (Fig.2).

359

360   4. 2. Chronostratigraphy, age-depth model and sedimentation accumulation rate

361 As shown in Table 1 and Figure 2, dates were obtained all along the core and generally fit with the

362 stratigraphy. Nevertheless, two age reversals are observed at the base of the core, based on Total Organic

363 Matter (TOM) measurements (Fig. 2). The first one occurs between 371.5 and 402 cm depth

364 (SacA44028) and the second corresponds to the bottom tephra layer of the core between 417.5 and 420.5

365 cm depth (SacA38523; Table 1). This could be attributed to stratigraphic misplacement or cross-

366 contamination during coring. Therefore, these dates were not included in the age model. All the wood

367 remain-based ages are very close to those from bulk TOM or slightly older (mean standard deviation

368 between the bulk TOM and the wood remain age is +2.3‰). This minor mismatch could be due to the

369 additional transport time of the wood remains from the catchment into the marsh sediment while the

370 bulk TOM signature is expected to be predominantly autochthonous (see sections 4.4 to 4.6).

371 Alternatively, "younger" TOM ages could result from microbial activity or organic matter derived from

372 root development occurring after sedimentation (Trumbore, 2009). The δ^{13}C values obtained after

373 sample preparation on residual CO_2 vary from -20.0‰ to -29.5‰ along the core (average value -25.3‰;

374 Tab. 1). This range is compatible with organic carbon originating from the vegetation, likely C3 type

375 plants, and consistent with δ^{13}C values measured at the nearby Lake Masoko (Gibert et al., 2002).

376 Compared to the mean TOM δ^{13}C value (-24.8‰), the mean wood δ^{13}C value is lower (-27.2‰) also in

377 agreement with a C3 type plant signature.

378 The investigated sediment sequence from Kyambangunguru shows continuous sedimentation of ca.

379 4080 calibrated years, spanning from ca. 4020 and -60 cal. BP (Fig. 2). The "apparent" sediment

380 accumulation rate (SAR) ranges from 0.03 to 0.18 cm yr^{-1} (i.e., each cm thick sample of the profile

381 records 6.3 to 33 years). The highest SAR was recorded in the bottom section of the profile (between

382 0.10 and 0.18 cm yr^{-1}), in the 417-191 cm section (from 4015 to 2280 cal. BP). Intermediate SAR values,

383 ranging between 0.07 and 0.11 cm yr^{-1}, were recorded between 191 and 8 cm (from 2280 to 130 cal.

384 BP), whereas the lowest SAR (0.03-0.06 cm yr^{-1}) was recorded in the top section of the profile between

385 8 and 0 cm (from 130 to -60 cal. BP). The σ error of the modelled dates ranged between 0.2 (top of the

386 profile) and 53 years.

387

388   4.3. Palynofacies

389 The Kyambangunguru core is largely dominated (ca. 80% of the OM throughout the core) by ligno-

390 cellulosic tissues (LC) from vascular plants (Fig. 3). Microscopic investigation of the LC reveals 3 stages

391 of degradation. On average, fresh, well-preserved, tLC tissues represent 19% of the total OM (Fig. 3),

392 while slightly degraded, saLC particles are the most abundant type of OM (ca. 39% on average) in the

393 core. Amorphous rAOM represents ca. 11% of the total LC OM with an increase to 20% in the section

394 from ca. 3140 to 830 cal. BP (300-62.5 cm). In addition to LC, fungal mycelia are observed in the layer

spanning the period between 239 and 60 cm (ca. 2670 to 800 cal. BP). Grey cell fragments and granular amorphous OM, related to planktonic-derived material, are found throughout the core (Fig. 3), but are particularly abundant at the base (below 330 cm, i.e. ca. 3360 cal. BP) and at the top of the profile (from 89.5 to 0 cm, ca. 1150 cal. BP to modern).

4.4. Plant macrofossil analysis

Plant macrofossils are dominated by macrophytes (sedges, submerged/floating plants and algae) and wood remains. *Eleocharis* sp. is present all along the core, while *Nymphaea* sp. (floating macrophyte), disappeared between 160 and 100 cm (ca. 1960 and 1270 cal. BP; Fig. 4). In addition, in the layer between 415.5 and 281.5 cm (ca. 4000 to 3000 cal. BP), macrofossils are composed of remains of algae (*Nitella* sp., Fig. 4) and submerged/floating plants (*Potamogeton* sp. and *Caldesia parnassiflora*; Fig. 4). These species are replaced by *Juncus* sp. from 239.5 to 139.5 cm (ca. 2670 to 1730 cal. BP). During this interval, there is a relative increase in abundance of wood remains in comparison to the other sections of the core. *Nitella* sp. together with *Carex* sp. and *Chara* sp. are the dominant remains found in the sequence from 139.5 to the surface (1730 cal. BP to modern; Fig. 4). At 105 cm (ca. 1330 cal. BP), *Aldrovanda vesiculosa* seed was found.

4.5. Pollen, NPPs and microcharcoal

265 taxa of pollen and spores as well as non-pollen palynomorphs (NPPs) – organic walled microfossils which are not pollen – were identified by palynological analysis. The results of this analysis were separated into two groups: indicators of terrestrial vegetation, i.e. vegetation surrounding the lake/marsh and indicators of aquatic vegetation reflecting mainly lake-marsh vegetation. Three pollen zones reflecting compositional changes in terrestrial (woodland and open land) communities (labelled as KY/tp-1 to -3 with tp: terrestrial pollen; Fig. 5) were defined. Additionally, the KY/tp-1 zone was subdivided into three subzones (KY/tp-1a-c). Pollen and NPPs reflecting lake/marsh vegetation changes enabled the establishment of 6 zones (KY/lpn-1-6 with lpn standing for local pollen and NPPs; Fig. 6).

4.5.1. Terrestrial vegetation

422   The KY/tp-1 zone (416–303 cm; ca. 4000–3160 cal. BP) is characteristic of the highest percentages of

423   *Acalypha*, Moraceae, *Macaranga* and *Piptadenia*/*Piptadeniastrum*/*Entada* (Fig. 5). Moraceae and

424   *Macaranga* pollen reached their maxima (27–28% and 11%, respectively) at 353-333 cm (ca. 3520–

425   3380 cal. BP). Poaceae pollen increased until 397 cm (ca. 3850 cal. BP) when they distinctly decreased

426   while Proteaceae pollen revealed a first maximum at 378 cm (ca. 3700 cal. BP). During the KY/tp-1b

427   subzone (353–333 cm; ca. 3520–3380 cal. BP), Poaceae percentages fell to their minimum values (8%).

428   During the KY/tp-1c subzone (333–303 cm; ca. 3380–3160 cal. BP) pollen values of Moraceae and

429   *Macaranga* dropped simultaneously with the rise in Poaceae percentages and the appearance of palm

430   pollen (*Elaeis guinensis* and *Raphia* type). During the entire KY/tp-1 zone charcoal (0.02–0.5 mm),

431   accumulation rate (CHAR) was high and relatively stable without any distinct maximum (8450–37940

432   particles cm^{-2} yr^{-1}; Fig. 5).

433   The KY/tp-2 zone (303–63 cm; ca. 3160–830 cal. BP) was characteristic of the highest values of *Uapaca*

434   (15–24%; 162.5-133.5 cm; ca. 1990–1660 cal. BP) in the profile. However, at 123–113.5 cm (ca. 1540–

435   1430 cal. BP) they substantially declined, simultaneously to a rapid increase in Poaceae values. At the

436   beginning of the zone, *Raphia* pollen increased rapidly (303–283 cm; ca. 3160–3010 cal. BP; up to

437   15.5%). Values of Proteaceae increased from 234.5 cm (ca. 2630 cal. BP) and reached the maxima after

438   113.5 cm (ca. 1430 cal. BP). Simultaneously, or slightly prior to the Poaceae maximum in this zone

439   (123–113.5 cm ca. 1540–1430 cal. BP), values of *Ricinus communis* and *Macaranga* increased (142.5

440   cm; ca. 1760 cal. BP), whereas percentages of *Nauclea* type (123 cm; ca. 1540 cal. BP), *Elaeis guinensis*

441   (143 cm; ca. 1770 cal. BP), *Raphia* type (132.5 cm; ca. 1650 cal. BP) and later Rutaceae (113.5 cm; ca.

442   1430 cal. BP) decreased substantially or disappeared. Among pollen taxa related to arboreal plants

443   occupying montane forest zones, *Apodytes* cf. *dimidiata*, *Olea*, *Podocarpus* and *Prunus africana* type

444   were the most common. During the KY/tp-2 zone, three distinct phases of increase in CHAR values,

445   potentially related to an increase in fire activity, were identified. These occurred at 297.5, 248.5 and

446   117.5 cm (ca. 3120, 2740, and 1480 cal. BP respectively) and were intersected by periods with CHAR

values lower than during the KY/tp-1 zone. From 83 cm (ca. 1070 cal. BP), CHAR values started to increase gradually.

The KY/tp-3 zone (63–5 cm; 830 to 60 cal. BP) was characterized by the highest percentages of Poaceae (67–90%), the continuous presence of *Ricinus communis* and distinct drops of Proteaceae and *Uapaca*. At 50 cm (ca. 690 cal. BP), *Syzygium* pollen value revealed a substantial increase (up to 16%). In general, CHAR values were higher than in the previous zone and two distinct maxima of their values were recorded at 50 and 10 cm (ca. 690 and 160 cal. BP).

4.5.2. Aquatic/marsh vegetation

During the KY/lpn-1 zone (416–383 cm; ca. 4000–3740 cal. BP) the algae *Tetraedron trigonum* type, *Tetraedron incus/caudatum* and *Coelastraum reticulatum* reached their maxima (Fig. 6). These algae taxa rapidly declined between 412 and 393 cm (ca 3970 and 3820 cal. BP). Along the KY/lpn-2 zone (383–303 cm; 3740–3160 cal. BP), Alismataceae (cf. *Caldesia*) was regularly observed (0.8–6.5%). Pollen of Nymphaeaceae (*Nymphaea* type) and their epidermis (UG-1241), *Potamogeton* and algae such as *Scenedesmus*, *Tetraedron minimum*, *Pediastrum* undiff., *Pediastrum angulosum* and *Botryococcus* were frequent during these two zones. At 323 cm (ca. 3310 cal. BP), *Nymphaea* type percentages increased simultaneously with a decline in *Potamogeton*. The KY/lpn-3 zone (303–193 cm; ca. 3160–2300 cal. BP) was characterized by an increase in Cyperaceae pollen and tissue fragment percentages (rise in fungal NPP UG-1176 and UG-1197) and a simultaneous drop in *Scenedesmus* and *Tetraedron minimum.*

The KY/lpn-4 zone (193–113 cm; ca. 2300–1430 cal. BP) was characterized by a prominent increase in Cyperaceae percentages (12–77%). The spores of *Lycopodiella caroliniana* were regularly present (0.2–18%) together with amoeba *Assulina muscorum*. Between 143 and 123 cm (ca. 1770 and 1540 cal. BP), monolete spores reached their maximum values in the core (64–69%). Values of *Nymphea* type, UG-1241 (*Nymphaea* tissues), *Potamogeton*, Alismataceae (cf. *Caldesia*), *Pediastrum angulosum*, *Botryococcus* and *Scenedesmus* dropped markedly. NPPs of fungal origin increased distinctly, notably UG-1197 and *Entorrhiza* in the deeper part of the zone and HdV-172, UG-1077, UG-1176 and UG-1107 in the upper part.

474   The KY/lpn-5 (113–46.5 cm; ca. 1430–650 cal. BP) and KY/lpn-6 (46.5–5 cm; 650 to 60 cal. BP) zones

475   were characterized by the increase in frequency of algae, mainly *Botryococcus*, *Scenedesmus* and

476   *Pediastrum angulosum* and, among submersed macrophytes, of *Nymphaea* type pollen and their related

477   tissues (UG-1241). In the KY/lpn-5 zone, Hallorrhagaceae appeared (1.5–24%). *Entorrhiza* and fungal

478   type UG-1107 reached maxima in the profile (59–76%). In the KY/lpn-6 zone, Alismataceae (cf.

479   *Caldesia*) and *Potamogeton* became more frequent while Cyperaceae pollen percentages distinctly

480   dropped.

481

482   4.6. Elemental analysis

483   C_{org} content is high throughout the core (39.0 - 57.8%; mean 51.0% ± 6.2; Suppl. Table 1), except in the

484   tephra layer at the base of the core (5%). Total nitrogen (TN) varies from 1.5 to 3.6% except for the

485   tephra layer (0.2%). Slightly lower TN values are observed between 199.5 and 100 cm (ca. 2350 and

486   1270 cal. BP; ca. 2%, Suppl. Table 1) leading to higher C/N ratios that range from 16 to 38 (Fig. 7 and

487   Suppl. Table 1). In the other sections of the core, C/N ratios are relatively invariant at ca. 15.

488

489   4.7. Br GDGT abundance and distribution

490   Br GDGTs are abundant throughout the core (mean 121.5 ± 81.3 µg g^{-1} of dry wt. peat), with maximal

491   concentration observed at 150.5 cm (ca. 1850 cal. BP; Suppl. Table 1). CBT varies between 0.53 and

492   2.01 with a mean value of 1.31 and is higher above 180.5 cm (ca. 2180 cal. BP; 1.41-2.01; Suppl. Table

493   1). MBT is comprised between 0.65 and 0.89, with a mean value of 0.77 (Suppl. Table 1). The highest

494   MBT values (>0.80) are found between 194 and 45 cm (ca. 2310 and 630 cal. BP).

495

496   4.8. *n*-Alkane distribution and their δ²H composition

497   Mid- to long-chain *n*-alkanes (>C_{21}) dominate most of the samples, with C_{23} and C_{25} being the most

498   abundant (on average 23% and 21%, respectively; Suppl. Fig. 1). Two *n*-alkane distribution patterns are

499 observed in the core (Suppl. Fig. 1), defined as patterns A and B. Pattern A was identified in the sections

500 from 417 to 180 cm and from 30 cm to the surface (ca. 3670 -2300 cal. BP and ca. 430 cal. BP-modern

501 respectively). It is dominated by odd numbered n-alkanes, the most abundant one being C_{23}, with a

502 decreasing trend in relative abundance from C_{23} to C_{31}. Pattern B (Suppl. Fig. 1) was observed in the

503 sections from 193 to 29.5 cm (ca. 2300 to 430 cal. BP). This distribution is characterized by a flattening

504 of the n-alkane profile. The C_{29}^{+} n-alkanes (up to C_{35} in some samples) as well as the C_{23}^{-} n-alkanes,

505 especially C_{19}, increase while the C_{23}, C_{25} and C_{27} decrease, in comparison to pattern A. In pattern B,

506 even numbered n-alkanes are also found in larger amount than in pattern A.

507 The CPI index confirms a strong odd-over-even predominance throughout the core (mean 8.1 ± 3; Suppl.

508 Table 2) while the ACL index varies between ca. 25 and 27 (Fig. 7; Suppl. Table 2). The P_{aq} index is

509 systematically higher than 0.4, ranging between 0.50 and 0.85 (Fig. 7; Suppl. Table 2).

510 The δ^2H values of odd mid to long chain n-alkanes (C_{23}-C_{31}) varies between -96‰ and -172‰ (Suppl.

511 Table 2) and are higher in the deepest part of the core, between 417 and 391 cm (ca. 4010 and 3800 cal.

512 BP; between -96‰ and -122‰; Suppl. Table 2). Long chain n-alkanes (C_{29} and C_{31}) are more ^{2}H-

513 enriched (-130‰ on average; Suppl. Table 2) than mid chain (C_{23} and C_{25}; -150‰ on average; Suppl.

514 Table 2) compounds.

515

516 **5. Discussion**

517 The combination of palaeobotanical, elemental and molecular analyses enabled the reconstruction of the

518 Holocene ecological history of the Kyambangunguru wetland together with regional climate. The proxy

519 analyses revealed the presence of three major phases in the Kyambangunguru wetland ecosystem

520 development over the last 4.0 ka cal. BP for which the interaction with regional and global climatic

521 changes are discussed. The chronology of the sediment record was compared to published records of

522 the region (Filippi and Talbot, 2005; Fontijn et al., 2012; Garcin et al., 2007) showing overall good

523 consistency. The tephra layer at the base of the core, dated at ca. 4.1 ka cal. BP, corresponds to the

524 Rungwe Pumice deposits identified at Lakes Masoko and Malawi and dated at 4.3 ka cal. BP and 4.3 to

525   3.6 ka cal. BP, respectively. The second tephra observed at ca. 0.9 ka cal. BP in the Kyambangunguru

526   core can be related to the Aphyric Pumice deposits observed at 1.2 ka cal. BP in the Lake Masoko

527   sediment record and between 1.1 and 0.6 ka cal. BP in the Lake Malawi one. The last tephra layer

528   identified at Kyambangunguru is harder to define. It is dated at ca. 0.8 ka cal. BP and could either

529   correspond to the Aphyric Pumice described earlier or to the Ngozi Tuff, even though this event was

530   dated between 0.5 and 0.3 ka cal. BP at Lakes Masoko and Malawi. This regional comparison, even if

531   it stresses its inherent time uncertainty, further validates the age-model used in this study.

532

533   5.1. Ecosystem, air temperature and precipitation variability at the Kyambangunguru crater marsh

534   Three units (labelled as Units I-III; Fig. 7), representing the major developmental phases of marshland

535   ecosystem over the last 4.0 ka cal. BP, were distinguished based on the local plant community changes

536   inferred from pollen, non-pollen palynomorph and plant macro-fossil analyses. In addition, the origin

537   of the OM and its degree of preservation were determined using the palynofacies and C/N records

538   (Bourdon et al., 2000) while the distribution of br GDGTs allowed reconstructing the pH of the site,

539   following the approach described by Weijers et al. (2007b) and Tierney et al. (2010b). For the climatic

540   reconstruction, the mean annual air temperature (MAAT) and the hydrological conditions over the last

541   4.0 ka cal. BP years were reconstructed using the br GDGT distribution and the hydrogen isotopic values

542   of the n-alkanes (δ^2H_{wax}), respectively. Br GDGT-derived MAAT were calculated with the East African

543   lacustrine calibration developed by Loomis et al. (2012), i.e. Eq. 7, which takes into account *in situ*

544   production of br GDGTs in lakes, as discussed in the Suppl. Information. The δ^2H_{wax} was determined as

545   the weighted average of the δ^2H values of the C_{23} and the C_{25} n-alkanes which are expected to have

546   recorded mainly the wetland water isotopic composition (δ^2H-H_2O) variations during the accumulation

547   of the sedimentary sequence (as discussed in the Suppl. Information). Because the study site has no

548   outflows, the δ^2H-H_2O variations depend essentially on the rates of precipitation and evaporation and

549   the δ^2H_{wax} can be interpreted as changes in the precipitation to evaporation ratio (P/E ratio; Gonfiantini,

550   1986; Sachse et al., 2004).

551

5.1.1. Unit I: ca. 4.0 – 2.3 ka cal. BP (417–193 cm) – shallow lake, cold and wet conditions

The palaeoenvironmental proxies suggest a relatively stable and persistent lake environment during this period. Planktonic remains are observed in the palynofacies (Fig. 3) and in the non-pollen palynomorph profile (NPP; Fig. 6) and the C/N values (ca. 15; Fig. 7) indicate a mixed aquatic and terrestrial source of the OM (Meyers, 1997). The GDGT derived-pH of ca. 7 (Fig. 7) is consistent with current pH values of the RVP crater lakes (ranging between 5.8 and 8.7; Delalande, 2008), further supporting the occurrence of a lake at this time. The high abundance of macro- and microremains (Figs. 4 and 6) from algae (*Nitella* sp.) and submerged/floating macrophytes (*Potamogeton* sp. and *Nymphaea* sp.) and the relatively high P_{aq} values (0.7-0.8; Ficken et al., 2000) suggest that the lake was relatively shallow and its water column likely harboured abundant macrophyte vegetation. The growth of *Caldesia parnassifolia* for instance may indicate a water depth lower than one meter (Gupta and Beentje, 2017; Sinkevičienė, 2016). In addition, the NPP record reveals a characteristic pattern of successive and rapid decline of *Tetraedron trigonum* type, *Coelastrum reticulatum* and *Tetraedron incus/caudatus*, all before 3.8 ka cal. BP (Fig. 6). This reduction is possibly related to the spread of *Nymphaea* whose floating leaves may have limited the light availability, although it did not seem to impact *Tetraedron minimum* and *Scenedesmus,* which might be more resistant species. The second stage of microalgal community retreat, which affected *Scenedesmus* and *Tetraedron minimum*, occurred at ca. 3.2 ka cal. BP and seem to have also been stimulated by *Nymphaea* expansion. Simultaneously, an increased input of fungal remains, UG-1176 and UG-1197, may indicate spreading of emerged marsh plants around the lake. This is further supported by the high C_{org} values (> 50%; Suppl. Table 1) and the predominance of lignocellulosic-derived OM in the palynofacies record partly originating from *Cyperus* (Laggoun-Défarge et al., 2008a) according to microscopic observation (Fig. 3).

Unit I is marked by an abrupt decrease in mean annual air temperature (MAAT) of about three degrees (from 26 °C to 23 °C, Fig. 8) at ca. 3.9 ka cal. BP. The MAAT continues to decrease by another three degrees to 20 °C at 2.7 ka cal. BP (Fig. 8). This trend is synchronous with the "3.3–2.5 ka. BP" cold Holocene event introduced by Wanner et al. (2011) which was also observed – to a lower extent – at ca.

578   4.0 – 3.0 ka cal. BP in Lakes Tanganyika and Malawi (Powers et al., 2005; Tierney et al., 2008; Fig. 8)

579   and in Lakes Turkana and Challa (Berke et al., 2012;

580   Sinninghe Damsté et al., 2012). At the same time, the δ^2H_{wax} record shows more negative values until

581   ca. 3.0 ka cal. BP (up to -168 ‰; Fig. 9), which can be interpreted as an increase in the P/E ratio either

582   due to higher precipitation or/and lower evaporation rates. A wetter environment is also inferred from

583   the terrestrial pollens, with a decrease in pollen supply from grassland communities from ca. 3.7 to 3.4

584   ka cal. BP and an expansion of mountain forest and Zambezian Miombo woodland communities

585   (Moraceae and *Macaranga* at ca. 3.5 – 3.4 ka cal. BP, *Uapaca* optimum, presence of *Apodytes cf.*

586   *dymidata*, *Olea*, *Podocarpus* and *Prunus africana)*. Wetter conditions at the same period were also

587   inferred from a pollen record at Lake Masoko (Vincens et al., 2003). Notably, a synchronous *Uapaca*

588   pollen optimum occurred both at Masoko and Kyambangunguru (after ca. 3.1 ka cal. BP, Vincens et al.,

589   2003). δ^2H_{wax} values remain negative during unit I, although two positive peaks in δ^2H_{wax} are noticeable

590   at ca. 3.6 and 2.8 ka cal. BP possibly indicating brief dry events interrupting the overall wetter period.

591   These dry events are in agreement with observations by Russell et al. (2003) and Russell and Johnson

592   (2005) at Lake Edward (Uganda; Fig. 9). Peaks in Mg content in calcite at 3.6 and 2.8 ka cal. BP were

593   indeed linked to evaporative concentration of the lake (increase in the $[Mg^{2+}]/[Ca^{2+}]$ ratio in lake water)

594   in response to short but pronounced drought events.

595   *5.1.2. Unit II: 2.3 – 1.4 ka cal. BP (193–113 cm) – marsh/peatland formation under sustained warm*

596   *and drier conditions*

597   An abrupt, environmental change occurred at ca. 2.3 ka cal. BP leading to the establishment of a peatland

598   with variable hydrological conditions (Fig. 7). The onset of unit II is marked by an apparent decrease in

599   the sedimentation rate from 0.13 cm yr^{-1} to 0.08 cm yr^{-1} (Fig. 2), an increase in the Cyperaceae tissue

600   and ferns (monolete spores) accumulation and a strong increase of the C/N ratio (up to 40), all

601   evidencing peat soil formation. High C/N ratios (usually > 30 and sometimes up to 100) are indeed

602   typical for peatlands, due to the high preservation of the OM in relation to the prevailing acidic and

603   anoxic conditions (Laggoun-Défarge et al., 2008b; Meyers, 1997). Simultaneously, a substantial

604   decrease or almost total disappearance of algae (*Scenedesmus*, *Pediastrum*, *Botryococcus* and

605 *Tetraedron minimum*) and aquatic plants such as *Nymphaea* spp. (Fig. 6) reflect a substantial fall in the

606 water table. However, irregular appearances of these taxa, as well as of the macroalgae *Nitella sp.*,

607 indicate episodic inundation of the wetland (Fig. 4). The main constituents of the peatland community

608 were *Juncus* sp., *Eleocharis* sp., ferns and perhaps other Cyperaceae species (Figs. 4 and 6). Permanent

609 waterlogged conditions, and low pH (down to 5.2, Fig. 7) contributed to the establishment of plant taxa

610 restricted to humid acidic environments, such as *Drosera*, *Lycopodiella caroliniana* and *Aldrovanda*

611 *vesiculosa* (Figs. 4 and 6; (Gałka et al., 2015), and the appearance of protists frequently found in

612 peatlands, such as the testate amoeba *Assulina muscorum* (van Geel, 1978). The increase in reddish

613 amorphous OM (rAOM) and the appearance of fungal mycelia at that time (Fig. 3) also suggest the start

614 of a terrestrialization process and the development of vascular plants within the marsh (Bourdon et al.,

615 2000). The increase in wood remains in the macrofossil profile, related to the development of trees and

616 shrubs at the edges of the marsh or even in the marsh itself, supports this interpretation.

617 Unit II displays the highest $\delta^2 H_{wax}$ values of the core (up to -136 ‰; Fig. 9), suggesting low P/E ratio

618 and thus the driest period of the last 4.0 ka cal. BP, consistent with several East-African records – Lake

619 Edward (Uganda), Lake Turkana (Kenya), Lake Tanganyika (Tanzania) (Nash et al., 2016 and

620 references therein). A major drought event is widely described at ca. 2.0 ka cal. BP, followed by a second

621 period between ca. 1.7 and 1.0 ka cal. BP, during which successive minor drought events occurred (Alin

622 and Cohen, 2003; Russell et al., 2007; Russell and Johnson, 2005; Verschuren and Charman, 2008). In

623 the Kyambangunguru $\delta^2 H_{wax}$ record, a positive excursion that could be interpreted as a drought event is

624 observed at ca. 2.2 ka cal. BP. However, the major dry period seems to have occurred later, between ca.

625 1.7 and 1.4 ka cal. BP (centred at 1.5 ka cal. BP, Fig. 9). Around the same time (ca. 1.7 ka cal. BP),

626 *Uapaca* pollen suddenly declined and fire activity increased, which contributed to the opening of the

627 woodland canopy and a spread of the grassland communities (Fig. 5). The same abrupt changes are

628 noticeable in charcoal and pollen data at Lake Masoko (Thevenon et al., 2003; Vincens et al., 2003) and

629 in the Amboseli basin in Kenya (Rucina et al., 2010). Alternatively, these vegetation changes could have

630 been induced by enhanced human activity. Indeed, a first spread of human settlement is considered to

631 have occurred during the Late Iron Age, around 1.5 ka cal. BP (Marchant and Taylor, 1998; Vincens et

632 al., 2003). However, several sites in East Africa (Lakes Turkana, Tanganyika, Naivasha, Challa, Edward

and Sacred Lake; see references in Marchant et al., 2018) support a widespread increase in aridity as the main cause explaining the sedimentological evidence of droughts, as discussed by Marchant et al. (2018). Notably, we promote that δ^2H_{wax} records, such as this study and Konecky et al. (2014), could help disentangling the human impact from the climatic one as they should only be marginally impacted by human activities. According to the br GDGT data, MAAT remained high during unit II, oscillating around 21.5-22 °C (Fig. 8), suggesting a dry and warm period during unit II. During the same period, higher temperatures are also reported in the records from Lake Challa (Sinninghe Damsté et al., 2012), Lake Turkana (Berke et al., 2012) and Lake Tanganyika (Tierney et al., 2008) (Fig. 8).

5.1.3. Unit III: ca. 1.4 ka cal. BP – modern (113–0 cm) – periodically flooded marsh and transition to colder conditions

At the onset of Unit III, an increase in the water table led to the reappearance of microalgae assemblages (mainly composed of *Botryococcus*, *Scenedesmus* and *Pediastrum angulosum*), and macrophytes such as *Nymphaea*, Alismataceae and Hallorrhagaceae at ca. 1.4 ka cal. BP. However, until ca. 0.7 ka cal. BP, high percentages of Cyperaceae and of *Entorrhiza* spores are observed, which indicate that the peatland was subjected to pronounced water table fluctuations but without open water stages. Indeed, *Entorrhiza* is a genus of parasites that infect the roots of the Juncaceae (rush) and Cyperaceae (sedge) families when they are no longer in water (Riess et al., 2015; Vánky, 1998). At ca. 0.7 ka cal. BP, the water table likely increased substantially, which supported a spread of *Nymphaea* and contributed to the sharp decrease in Cyperaceae. Since ca. 0.4 ka cal. BP, *Tetraedron minimum* and *Scenedesmus* blooms became more frequent, and the structure of the microalgal communities resembled the one from the base of the core (start of Unit I). This time, however, large amounts of *Carex* remains and large fluctuations in pH (from 5.2 to 7.8; Fig. 7) suggest the coexistence of peat patches, likely acidic, and water depressions where the pH may have been higher, supporting the development of microalgal communities. This corresponds to the current status of the marsh. Continuous monitoring of the site during the last decade indicates the presence of a seasonally evolving ecosystem, i.e. (i) a shallow lake colonized by large sedge mats during the rainy season and (ii) a waterlogged marsh-like regime at the end of the dry season due to high evaporation rates (Delalande et al., 2008a, 2008b).

The period that corresponds to unit III at Kyambangunguru starts with relatively warm mean annual air temperatures, at ca. 22 °C, followed by an abrupt cooling to 20 °C at ca. 0.5 ka cal. BP (Fig. 8). A similar abrupt event was also identified at Lake Tanganyika (Tierney et al., 2010a; Fig. 8), in the Ethiopian Highlands and in southern Africa (Nicholson et al., 2013 and references therein) and could coincide with the transition between a "Medieval Climate Anomaly" (MCA; based on Jones et al. (2001) time boundaries: ca. 1.0 – 0.8 ka cal. BP) and a Little Ice Age (LIA; 0.7 – 0.1 ka cal. BP; Matthews and Briffa, 2005) in the African continent. The occurrence of climatic shifts in Africa that could be related to the European MCA and LIA events is currently under debate but a growing body of research seems to support such a cross-latitude connection (e.g. Lüning et al., 2018; Russell and Johnson, 2007; Tierney et al., 2013). At Kyambangunguru, the last 500 yrs exhibit the coldest temperatures of the record which would support the existence of a "Little Ice Age" equivalent in East Africa, in agreement with records from nearby Lake Malawi (Branchu et al., 2010; Powers et al., 2011; Fig. 8). At the transition between units II and III (ca. 1.4 – 0.8 ka cal. BP) the δ^2H_{wax} values decrease, consistent with the reestablishment of higher P/E ratio under wetter conditions and the spreading of Proteaceae and the recovery of the *Uapaca* woodlands, as observed in the pollen record. At 0.8 ka cal. BP, the canopy density started to decrease, the fire activity increased, which led to a spread in the grassland communities, maintained until nowadays. Similar conditions were recorded at Lake Masoko (Vincens et al., 2003). Intensification of human activity in the region could be responsible for such vegetation changes, especially as no shift is observed in the δ^2H_{wax} values during this period. Additional high-resolution reconstructions in the RVP and the neighbouring provinces are necessary to better assess the relative contribution of human versus climatic nature of these recent environmental shifts.

5.2. Implications for climate dynamics in East Africa during the late Holocene and its impact on highland wetland ecology

The temperature and P/E ratio records at Kyambangunguru show a high variability over the last 4.0 ka cal. BP. The main two warm periods, before ca. 3.7 ka cal. BP and between ca. 2.2 and 1.0 ka cal. BP, were generally accompanied by drier conditions (Figs. 8 and 9). A major dry event at 4.2 ka cal. BP is

687   a common feature in many tropical and temperate records and was interpreted as a southward migration

688   of the ITCZ (e.g. Gasse, 2000; Mayewski et al., 2004). A severe drought has also been observed in many

689   other East African sites around 2.0 ka cal. BP (Marchant et al., 2018) and could have been related to the

690   dry and warm period centred at ca. 1.5 ka cal. BP at Kyambangunguru. The discrepancy in timing

691   between the RVP and the other tropical East African records may be related to the unique location of

692   the RVP at the southern end of the tropical climatic belt ($\approx$ 10 °S), i.e. at the transition between two

693   hydro-climatic regimes (the north-eastern and the southern ones). Two cold and wet periods were

694   identified, between ca. 3.3 and 2.0 ka cal. BP and since ca. 0.6 ka cal. BP. The latter period is concurrent

695   with the European Little Ice Age and suggests that this cold event may have occurred globally (e.g.

696   Brown and Johnson, 2005). The warm and dry period at ca. 1.5 ka cal. BP and the two cold and wet

697   events all correspond to cold periods identified by Wanner et al. (2011) supporting the idea that the

698   Holocene climatic variability is at least partly driven by global scale events (e.g. solar and volcanic

699   activities, changes in the thermohaline circulation). However, it emphasizes that these processes seemed

700   to have contrasting effects at different latitudes (cooling vs. warming).

701   A major ecological shift that led to the transition from a shallow lake to a peatland at Kyambangunguru

702   started at ca. 2.5 ka cal. BP, in a rather wet environment, 300 years before the δ^2H_{wax} exhibit an abrupt

703   shift towards drier conditions (Fig 9). This time offset suggests that the ecological change recorded at

704   Kyambangunguru was primarily due to a hydroseral succession, i.e. the natural progressive colonisation

705   and infilling of a freshwater lake by different types of macrophytes leading to its transition to a swamp

706   which could eventually turn into a forest (Charman, 2002). A drier peatland was established at ca. 2.2

707   ka cal. BP and sustained until ca. 1.4 ka cal. BP likely as a result of combined warm and dry conditions,

708   which significantly lowered the P/E ratio of the wetland (Fig. 8 and 9). This is consistent with the abrupt

709   change at ca. 2.2 ka cal. BP observed in the biotic communities: planktonic and *Nymphaea* communities

710   disappeared, while *Cyperus* spp. took over in only a century (Fig. 6). This behaviour suggests a threshold

711   effect, which may reflect an autogenic hydroseral development triggered by gradual warming

712   conditions. Previous studies have shown the ability of *Nymphaea* spp. to form mats floating at the

713   surface of the water (Charman, 2002; Ellery et al., 1990) and pointed it out as a common step in the

714   hydroseral succession leading to the conversion of a freshwater body to a swamp (Kratz and DeWitt,

715   1986; Swan and Gill, 1970). The development of floating mats could be accelerated in the tropics, as

716   the warm air temperatures hold up high vegetation productivity rates (Talling et al., 1998). The slight

717   warming recorded at ca. 2.6 ka cal. BP (by the br GDGTs; Fig. 8) could then have acted as a positive

718   feedback in promoting high rates of vegetation productivity. The consequences of this fast development

719   of floating mats are (i) large inputs of OM in the sediment, which progressively infilled the lake, (ii) a

720   vertical expansion of the mats by peat accumulation, and (iii) a horizontal expansion and partial covering

721   of the surface of the lake. From ca. 3.3 to 2.3 ka cal. BP (Fig. 6), opposite trends are observed in the

722   distribution of plankton and *Nymphaea* suggesting that the more *Nymphaea* mats would cover the lake

723   surface, the less light would penetrate the water column leading to a decrease in microalgae abundance,

724   supporting the proposed mechanism of lake infilling.

725   This terrestrialization process was interrupted at ca. 1.4 ka cal. BP, when pronounced fluctuations in the

726   water table are revealed by the presence of *Enthorriza* in the microfossil record (ca. 1.4 – 0.7 ka cal. BP;

727   Fig. 6). The water balance, recorded by the δ^2H_{wax}, increased over this period, suggesting a relative

728   increase in precipitation (Fig. 9) in agreement with the spread of Proteaceae and *Uapaca* in the terrestrial

729   pollen. This likely re-flooded the marsh and created patches of open water, where phytoplankton, and

730   then *Nymphaea*, could re-colonise the marsh (Fig. 6). A similar ecosystem change was encountered at

731   the same period in a mountainous marsh in Madagascar (Bourdon et al., 2000). This period of water

732   fluctuations, synchronous with the Medieval Climate Anomaly (MCA; 1.0 – 0.8 ka cal. BP), is the only

733   period of the investigating 4000 yr record when conditions were warm and wet at Kyambangunguru,

734   suggesting that its origin may be different from the other recorded climatic changes. The MCA is

735   described as warm and dry in most north-eastern Africa (Lüning et al., 2017; Nash et al., 2016;

736   Nicholson et al., 2013) and humid in southern Africa (e.g. Nash et al., 2016; Tyson and Lindesay, 1992;

737   Woodborne et al., 2015). A recent literature review by Lüning et al. (2018) suggests a transition zone

738   across Tanzania with increased signs of humidity along a NE-SW transect. Notably, Buckles et al.

739   (2016) and Finch et al. (2017) recorded wet conditions at Lake Challa until ca. 800 BP and at the

740   Kwasebuge peat bog until ca. 675 BP, respectively. Hence the Kyambangunguru record presented here

741   extends this transitional zone to the southeast, in agreement with the hydroclimatic interpretation of a

742   biogenic silica record by Johnson et al. (2004) at Lake Malawi.

743

6. Conclusions

The detailed multi-proxy analysis of a 4-m peat core covering the late Holocene (4000 years) reveals

rapid and profound ecological changes of the Kyambangunguru wetland in the Rungwe Volcanic

Province (RVP), southwestern Tanzania. Around 2.2 ka cal. BP, a shallow crater lake turned into a

peatland. Starting at ca. 0.9 ka cal. BP the water level in the marsh increased, creating a shallow lake

during the rainy season and a peaty marsh during the dry season. These significant ecological

fluctuations correlated with major changes of the Late Holocene East African climate. Notably, the air

temperatures remained high and the reconstructed precipitation low between ca. 2.2 and 0.9 ka cal. BP,

which allowed the peatland terrestrialization to sustain. This study represents the first detailed late

Holocene quantitative air temperature reconstruction from the RVP region. We identified a succession

of cold/warm/cold events, largely in phase with the other regional East African climate records and with

the cold periods identified worldwide by Wanner et al. (2011). This further supports that global scale

processes may be the main drivers of the Holocene climatic variability. Moreover, warm conditions

during the MCA followed by abrupt cooling during the LIA were observed at Kyambangunguru and

elsewhere in East Africa suggesting that these two recent events occurred globally. The precipitation

pattern at Kyambangunguru during these two events is opposite to most of the more north-eastern

African records and rather resembles the southern African climatic records. Recent additional

precipitation records in Tanzania also show such a pattern. Tanzania seemed thus to be located at the

transition zone between two hydro-climatic poles (north-eastern and southern Africa) and to have

experienced a variable relative contribution of these two poles over the last millennium. This study

further demonstrates that peatlands and marshes provide valuable, high resolution climatic archives in

the tropics that offer novel avenues of research for understanding linkages between the Holocene climate

variability and ecosystem change in the tropics.

767

768

780

781 **Figure and Table captions:**

782 Figure 1: Regional setting and climatic conditions of the studied site. A: geographical location of the

783 Rungwe Volcanic Province (RVP, adapted from Delalande, 2008), the green lines outline the maximal

784 positions of the intertropical convergence zone (ITCZ) over the year, the blue lines delimitate the

785 equatorial rain region and the histograms show the monthly mean precipitation values (mm) at the main

786 East African weather stations; B: topographical map of the RVP and location of the Kyambangunguru

787 marsh; C: lake level (black dots), precipitation (blue bars) and marsh water δ^2H composition (red dots)

788 variations over one calendar year; D-E: pictures of the Kyambangunguru crater marsh taken in July

789 2014.

790 Figure 2: Lithology (A) and Bayesian age-depth model (B). The A values indicate the agreement

791 between the modelled and the calibrated age and the A_{model} the agreement of the model itself. TOM

792 samples are in black, wood samples in red and tephra ones in grey. Horizontal dotted lines represent the

793 model boundaries (see text for details) and excluded dates are identified as outliers.

794   <u>Figure 3:</u> Quantitative palynofacies: relative abundance of the main organic aggregates analysed by

795   photonic microscopy in transmitted light. In green: ligno-cellulosic tissues (LC): (i) fresh LC detected

796   as translucent LC (tLC) in light green, (ii) slightly degraded/amorphised LC (saLC) in yellow-green and

797   (iii) totally degraded/amorphous LC, characterised by red aggregates of amorphous OM (rAOM) in dark

798   green. In orange: mycelium (myc) fragments. In blue: planktonic remains (algOM).

799   <u>Figure 4:</u> Plant macro-fossil diagram. Results are given in absolute numbers. For the legend of the

800   lithology column see Fig. 2. Roman numbers indicate the three ecological units as defined in the

801   discussion part.

802   <u>Figure 5:</u> Woodland pollen diagram for the Kyambangunguru marsh showing relative percentages of

803   the selected taxa. The grey pattern shows a 10x magnification. For the legend of the lithology column

804   see Fig. 2. Roman numbers indicate the three ecological units as defined in the discussion part.

805   <u>Figure 6:</u> Ferns, aquatic pollen and NPP diagram for the Kyambangunguru marsh showing relative

806   percentages of the selected taxa. The grey pattern shows a 10x magnification. For the legend of the

807   lithology column see Fig. 2. Roman numbers indicate the three ecological units as defined in the

808   discussion part.

809   <u>Figure 7:</u> Lithology (A; see details in Fig. 2), total organic carbon over total nitrogen atomic ratio (B),

810   br GDGT-derived pH (C; based on Tierney et al. (2010b) calibration) and n-alkane distribution indices

811   (D-E; ACL and Paq, respectively). The three units discussed in the text are also represented along with

812   their ecological interpretation.

813   <u>Figure 8:</u> (a) Lake Tanganyika TEX_{86}-derived lake surface temperature (LST) of the last 4000 (black

814   contour red dots) and 1500 (red plain dots) years (Tierney et al., 2010a and 2008 respectively) and (b)

815   Lake Malawi TEX_{86}-derived LST of the last 4000 (black contour yellow dots) and 700 (yellow plain

816   dots) years (Powers et al., 2005, 2011) compared to (c) Kyambangunguru br GDGT-derived MAAT

817   (present study). The three units described in the text are also represented (dashed lines).

818 Figure 9: (a) Lake Edward Mg (mol %; Russell and Johnson, 2005) and (b) Kyambangunguru δ²Hwax

819 records for the last 4000 years (present study). The three units described in the text are also represented

820 (dashed lines).

821 Table 1: AMS Radiocarbon chronology of the core KYAM12 (2012). Calibrated median age and range

822 (2σ) were obtained using OxCal 4.3 software (Bronk Ramsey and Lee, 2013) with the ShCal 13

823 atmospheric curve (Hogg et al., 2013) and Bomb13SH3 (Hua et al., 2013).

References:

825 Alin, S.R., Cohen, A.S., 2003. Lake-level history of Lake Tanganyika, East Africa, for the
826   past 2500 years based on ostracode-inferred water-depth reconstruction. Palaeogeogr.
827   Palaeoclimatol. Palaeoecol. 199, 31–49. https://doi.org/10.1016/S0031-
828   0182(03)00484-X
829 Amesbury, M.J., Barber, K.E., Hughes, P.D.M., 2012. Can rapidly accumulating Holocene
830   peat profiles provide sub-decadal resolution proxy climate data? J. Quat. Sci. 27, 757–
831   770. https://doi.org/10.1002/jqs.2561
832 Basalirwa, C. p. k., Odiyo, J. o., Mngodo, R. j., Mpeta, E. j., 1999. The climatological regions
833   of Tanzania based on the rainfall characteristics. Int. J. Climatol. 19, 69–80.
834   https://doi.org/10.1002/(SICI)1097-0088(199901)19:1<69::AID-JOC343>3.0.CO;2-M
835 Berglund, B.E., Ralska-Jasiewiczowa, M., 1986. Handbook of Holocene Palaeoecology and
836   Palaeohydrology, J. Wiley & Sons Ltd. ed. Berglund, B.E., Ralska- Jasiewiczowa, M.,
837   Chichester-Toronto.
838 Berke, M.A., Johnson, T.C., Werne, J.P., Schouten, S., Sinninghe Damsté, J.S., 2012. A mid-
839   Holocene thermal maximum at the end of the African Humid Period. Earth Planet. Sci.
840   Lett. 351, 95–104. https://doi.org/10.1016/j.epsl.2012.07.008
841 Blackford, J., 2000. Palaeoclimatic records from peat bogs. Trends Ecol. Evol. 15, 193–198.
842   https://doi.org/10.1016/S0169-5347(00)01826-7
843 Bonnefille, R., Roeland, J.C., Guiot, J., 1990. Temperature and rainfall estimates for the past
844   40,000 years in equatorial Africa. Nature 346, 347. https://doi.org/10.1038/346347a0
845 Bourdon, S., Laggoun-Défarge, F., Disnar, J.-R., Maman, O., Guillet, B., Derenne, S.,
846   Largeau, C., 2000. Organic matter sources and early diagenetic degradation in a
847   tropical peaty marsh (Tritrivakely, Madagascar). Implications for environmental
848   reconstruction during the Sub-Atlantic. Org. Geochem. 31, 421–438.
849 Boussafir, M., Sifeddine, A., Jacob, J., Foudi, M., Cordeiro, R.C., Albuquerque, A.L.S.,
850   Abrao, J.J., Turcq, B., 2012. Petrographical and geochemical study of modern
851   lacustrine sedimentary organic matter (Lagoa do Caçò, Maranão, Brazil): Relationship
852   between early diagenesis, organic sedimentation and lacustrine filling. Org. Geochem.
853   47, 88–98. https://doi.org/10.1016/j.orggeochem.2012.03.013
854 Branchu, P., Bergonzini, L., Delvaux, D., De Batist, M., Golubev, V., Benedetti, M., Klerkx,
855   J., 2005. Tectonic, climatic and hydrothermal control on sedimentation and water
856   chemistry of northern Lake Malawi (Nyasa), Tanzania. J. Afr. Earth Sci. 43, 433–446.
857   https://doi.org/10.1016/j.jafrearsci.2005.09.004
858 Branchu, P., Bergonzini, L., Pons-Branchu, E., Violier, E., Dittrich, M., Massault, M.,
859   Ghaleb, B., 2010. Lake Malawi sediment and pore water chemistry: Proposition of a
860   conceptual model for stratification intensification since the end of the Little Ice Age.

Glob. Planet. Change, Quaternary and Global Change: Review and Issues Special issue in memory of Hugues FAURE 72, 321–330. https://doi.org/10.1016/j.gloplacha.2010.01.008

Bray, E.E., Evans, E.D., 1961. Distribution of *n*-paraffins as a clue to recognition of source beds. Geochim. Cosmochim. Acta 22, 2–15. https://doi.org/10.1016/0016-7037(61)90069-2

Bronk Ramsey, C.B., 1995. Radiocarbon calibration and analysis of stratigraphy: The OxCal program. Radiocarbon 37, 425–430. https://doi.org/10.1017/S0033822200030903

Bronk Ramsey, C.B., 2008. Deposition models for chronological records. Quat. Sci. Rev., INTegration of Ice-core, Marine and Terrestrial records (INTIMATE): Refining the record of the Last Glacial-Interglacial Transition 27, 42–60. https://doi.org/10.1016/j.quascirev.2007.01.019

Bronk Ramsey, C.B., 2009. Bayesian analysis of radiocarbon dates. Radiocarbon 51, 337–360. https://doi.org/10.1017/S0033822200033865

Bronk Ramsey, C.B., Lee, S., 2013. Recent and planned developments of the program OxCal. Radiocarbon 55, 720–730. https://doi.org/10.1017/S0033822200057878

Brown, E.T., Johnson, T.C., 2005. Coherence between tropical East African and South American records of the Little Ice Age. Geochem. Geophys. Geosystems 6, Q12005. https://doi.org/10.1029/2005GC000959

Buckles, L.K., Verschuren, D., Weijers, J.W.H., Cocquyt, C., Blaauw, M., Sinninghe Damsté, J.S., 2016. Interannual and (multi-)decadal variability in the sedimentary BIT index of Lake Challa, East Africa, over the past 2200 years: assessment of the precipitation proxy. Clim Past 12, 1243–1262. https://doi.org/10.5194/cp-12-1243-2016

Chambers, F.M., Booth, R.K., De Vleeschouwer, F., Lamentowicz, M., Le Roux, G., Mauquoy, D., Nichols, J.E., van Geel, B., 2012. Development and refinement of proxy-climate indicators from peats. Quat. Int., Peat Stratigraphy and Climate Change 268, 21–33. https://doi.org/10.1016/j.quaint.2011.04.039

Charman, D., 2002. Peatlands and Environmental Change, John Wiley & Sons. ed. England.

Coffinet, S., Huguet, A., Williamson, D., Bergonzini, L., Anquetil, C., Majule, A., Derenne, S., 2015. Occurrence and distribution of glycerol dialkanol diethers and glycerol dialkyl glycerol tetraethers in a peat core from SW Tanzania. Org. Geochem. 83–84, 170–177. https://doi.org/10.1016/j.orggeochem.2015.03.013

Coffinet, S., Huguet, A., Pedentchouk, N., Bergonzini, L., Omuombo, C., Williamson, D., Anquetil, C., Jones, M., Majule, A., Wagner, T., Derenne, S., 2017. Evaluation of branched GDGTs and leaf wax n-alkane δ2H as (paleo) environmental proxies in East Africa. Geochim. Cosmochim. Acta 198, 182–193. https://doi.org/10.1016/j.gca.2016.11.020

Cottereau, E., Arnold, M., Moreau, C., Baqué, D., Bavay, D., Caffy, I., Comby, C., Dumoulin, J.-P., Hain, S., Perron, M., Salomon, J., Setti, V., 2007. Artemis, the new ^{14}C AMS at LMC14 in Saclay, France. Radiocarbon 49, 291–299. https://doi.org/10.1017/S0033822200042211

Davis, M.B., Deevey Jr., E.S., 1964. Pollen accumulation rates: estimates from late-glacial sediment of Rogers Lake. Science 145, 1293–1295.

Delalande, M., 2008. Hydrologie et géochimie isotopique du lac Masoko et de lacs volcaniques de la province active du Rungwe (Sud-Ouest Tanzanie). Université Paris Sud-Paris XI.

Delalande, M., Bergonzini, L., Branchu, P., Filly, A., Williamson, D., 2008a. Hydroclimatic and geothermal controls on the salinity of Mbaka Lakes (SW Tanzania): Limnological and paleolimnological implications. J. Hydrol. 359, 274–286. https://doi.org/10.1016/j.jhydrol.2008.07.007

Delalande, M., Bergonzini, L., Massault, M., 2008b. Mbaka lakes isotopic (18O and 2H) and water balances: discussion on the used atmospheric moisture compositions. Isotopes Environ. Health Stud. 44, 71–82. https://doi.org/10.1080/10256010801887414

Eglinton, G., Hamilton, R.J., 1967. Leaf epicuticular waxes. Science, New Series 156, 1322–1335.

Ellery, K., Ellery, W.N., Rogers, K.H., Walker, B.H., 1990. Formation, colonization and fate of floating sudds in the Maunachira river system of the Okavango Delta, Botswana. Aquat. Bot. 38, 315–329. https://doi.org/10.1016/0304-3770(90)90027-I

Estep, M., Hoering, T., 1980. Biogeochemistry of the stable hydrogen isotopes. Geochim. Cosmochim. Acta 44, 1197–1206. https://doi.org/10.1016/0016-7037(80)90073-3

Ficken, K.J., Li, B., Swain, D.L., Eglinton, G., 2000. An n-alkane proxy for the sedimentary input of submerged/floating freshwater aquatic macrophytes. Org. Geochem. 31, 745–749. https://doi.org/10.1016/S0146-6380(00)00081-4

Filippi, M.L., Talbot, M.R., 2005. The palaeolimnology of northern Lake Malawi over the last 25 ka based upon the elemental and stable isotopic composition of sedimentary organic matter. Quat. Sci. Rev. 24, 1303–1328. https://doi.org/10.1016/j.quascirev.2004.10.009

Finch, J., Marchant, R., Courtney Mustaphi, C.J., 2017. Ecosystem change in the South Pare Mountain bloc, Eastern Arc Mountains of Tanzania. The Holocene 27, 796–810. https://doi.org/10.1177/0959683616675937

Finsinger, W., Tinner, W., 2005. Minimum count sums for charcoal concentration estimates in pollen slides: accuracy and potential errors. The Holocene 15, 293–297.

Fontijn, K., Ernst, G.G.J., Elburg, M.A., Williamson, D., Abdallah, E., Kwelwa, S., Mbede, E., Jacobs, P., 2010. Holocene explosive eruptions in the Rungwe Volcanic Province, Tanzania. J. Volcanol. Geotherm. Res. 196, 91–110. https://doi.org/10.1016/j.jvolgeores.2010.07.021

Fontijn, K., Williamson, D., Mbede, E., Ernst, G.G.J., 2012. The Rungwe Volcanic Province, Tanzania – A volcanological review. J. Afr. Earth Sci. 63, 12–31. https://doi.org/10.1016/j.jafrearsci.2011.11.005

Gałka, M., Bergonzini, L., Williamson, D., Majule, A., Masao, C., Huguet, A., 2015. Macrofossil evidence of Late Holocene presence of Aldrovanda vesiculosa L. in Central-Eastern Europe (Poland) and East Africa (Tanzania). Quat. Int., Palaeolandscapes from Saalian to Weichselian: INQUA TERPRO Commission, Peribaltic International Field Symposium, Lithuania 386, 186–190. https://doi.org/10.1016/j.quaint.2015.05.058

Garcin, Y., Williamson, D., Taieb, M., Vincens, A., Mathé, P.-E., Majule, A., 2006. Centennial to millennial changes in maar-lake deposition during the last 45,000 years in tropical Southern Africa (Lake Masoko, Tanzania). Palaeogeogr. Palaeoclimatol. Palaeoecol. 239, 334–354. https://doi.org/10.1016/j.palaeo.2006.02.002

Garcin, Y., Williamson, D., Bergonzini, L., Radakovitch, O., Vincens, A., Buchet, G., Guiot, J., Brewer, S., Mathé, P.-E., Majule, A., 2007. Solar and anthropogenic imprints on Lake Masoko (southern Tanzania) during the last 500 years. J. Paleolimnol. 37, 475–490. https://doi.org/10.1007/s10933-006-9033-6

Gasse, F., 2000. Hydrological changes in the African tropics since the Last Glacial Maximum. Quat. Sci. Rev. 19, 189–211. https://doi.org/10.1016/S0277-3791(99)00061-X

Gelorini, V., Verbeken, A., van Geel, B., Cocquyt, C., Verschuren, D., 2011. Modern non-pollen palynomorphs from East African lake sediments. Rev. Palaeobot. Palynol. 164, 143–173. https://doi.org/10.1016/j.revpalbo.2010.12.002

Gibert, E., Bergonzini, L., Massault, M., Williamson, D., 2002. AMS-^{14}C chronology of 40.0 cal ka BP continuous deposits from a crater lake (Lake Massoko, Tanzania): Modern

water balance and environmental implications. Palaeogeogr. Palaeoclimatol. Palaeoecol. 187, 307–322. https://doi.org/10.1016/S0031-0182(02)00483-2

Gonfiantini, R., 1986. Chapter 3 - Environmental isotopes in lake studies, in: Fritz, P., Fontes, J.C. (Eds.), The Terrestrial Environment, B, Handbook of Environmental Isotope Geochemistry. Elsevier, Amsterdam, pp. 113–168. https://doi.org/10.1016/B978-0-444-42225-5.50008-5

Gosling, W.D., Miller, C.S., Livingstone, D.A., 2013. Atlas of the tropical West African pollen flora. Rev. Palaeobot. Palynol. Palynology of tropical Africa 199, 1–135. https://doi.org/10.1016/j.revpalbo.2013.01.003

Graz, Y., Di-Giovanni, C., Copard, Y., Laggoun-Défarge, F., Boussafir, M., Lallier-Vergès, E., Baillif, P., Perdereau, L., Simonneau, A., 2010. Quantitative palynofacies analysis as a new tool to study transfers of fossil organic matter in recent terrestrial environments. Int. J. Coal Geol. 84, 49–62. https://doi.org/10.1016/j.coal.2010.08.006

Gupta, A.K., Beentje, H.J., 2017. Caldesia parnassifolia. The IUCN Red List of Threatened Species 2017: e.T162381A83996588.

Han, D., Ha, H.K., Hwang, C.Y., Lee, B.Y., Hur, H.-G., Lee, Y.K., 1968. Bacterial distribution along stratified water Columns in the pacific sector of the Arctic ocean. Deep Sea Res. Part II Top. Stud. Oceanogr. https://doi.org/10.1016/j.dsr2.2014.06.007

Hogg, A.G., Hua, Q., Blackwell, P.G., Niu, M., Buck, C.E., Guilderson, T.P., Heaton, T.J., Palmer, J.G., Reimer, P.J., Reimer, R.W., Turney, C.S.M., Zimmerman, S.R.H., 2013. SHCal13 Southern Hemisphere Calibration, 0–50,000 Years cal BP. Radiocarbon 55, 1889–1903. https://doi.org/10.2458/azu_js_rc.55.16783

Hua, Q., Barbetti, M., Rakowski, A.Z., 2013. Atmospheric radiocarbon for the period 1950–2010. Radiocarbon 55, 2059–2072. https://doi.org/10.2458/azu_js_rc.v55i2.16177

Johnson, T.C., Brown, E.T., McManus, J., 2004. Diatom productivity in northern Lake Malawi during the past 25,000 years: Implications for the position of the intertropical convergence zone at millennial and shorter time scales, in: Battarbee, R.W., Gasse, F., Stickley, C.E. (Eds.), Past climate variability through Europe and Africa. Springer, Dordrecht, pp. 93–116.

Jones, P.D., Osborn, T.J., Briffa, K.R., 2001. The evolution of climate over the last Millennium. Science 292, 662–667. https://doi.org/10.1126/science.1059126

Killops, V., Killops, S., 2005. Introduction to organic geochemistry 2d edition. Blackwel Publishing Ltd.

Konecky, B., Russell, J., Huang, Y., Vuille, M., Cohen, L., Street-Perrott, F.A., 2014. Impact of monsoons, temperature, and CO_2 on the rainfall and ecosystems of Mt. Kenya during the Common Era. Palaeogeogr. Palaeoclimatol. Palaeoecol. 396, 17–25. https://doi.org/10.1016/j.palaeo.2013.12.037

Kratz, T.K., DeWitt, C.B., 1986. Internal factors controlling peatland-lake ecosystem development. Ecology 67, 100–107. https://doi.org/10.2307/1938507

Laggoun-Défarge, F., Mitchell, E., Gilbert, D., Disnar, J.-R., Comont, L., Warner, B.G., Buttler, A., 2008a. Cut-over peatland regeneration assessment using organic matter and microbial indicators (bacteria and testate amoebae). J. Appl. Ecol. 45, 716–727.

Laggoun-Défarge, F., Gilbert, D., Buttler, A., Epron, D., Francez, A.-J., Grasset, L., Mitchell, E.A.D., Guimbaud, C., Roy, J.-C., 2008b. Effects of experimental warming on carbon sink function of a temperate pristine mire : the PEATWARM project. in: International Peat Society Congress. Tullamore, Irlande.

Loisel, J., Yu, Z., 2013. Surface vegetation patterning controls carbon accumulation in peatlands. Geophys. Res. Lett. 40, 5508–5513. https://doi.org/10.1002/grl.50744

Loomis, S.E., Russell, J.M., Ladd, B., Street-Perrott, F.A., Sinninghe Damsté, J.S., 2012. Calibration and application of the branched GDGT temperature proxy on East African

1011   lake sediments. Earth Planet. Sci. Lett. 357–358, 277–288.
1012   https://doi.org/10.1016/j.epsl.2012.09.031

1013 Loomis, S.E., Russell, J.M., Lamb, H.F., 2015. Northeast African temperature variability
1014   since the Late Pleistocene. Palaeogeogr. Palaeoclimatol. Palaeoecol. 423, 80–90.
1015   https://doi.org/10.1016/j.palaeo.2015.02.005

1016 Lüning, S., Gałka, M., Vahrenholt, F., 2017. Warming and cooling: the medieval climate
1017   anomaly in Africa and Arabia. Paleoceanography 32, 2017PA003237.
1018   https://doi.org/10.1002/2017PA003237

1019 Lüning, S., Gałka, M., Danladi, I.B., Adagunodo, T.A., Vahrenholt, F., 2018. Hydroclimate in
1020   Africa during the Medieval Climate Anomaly. Palaeogeogr. Palaeoclimatol.
1021   Palaeoecol. 495, 309–322. https://doi.org/10.1016/j.palaeo.2018.01.025

1022 Majule, A.E., 2010. The impact of land management practices on soil quality and implications
1023   on smallholder productivity. Environ. Econ. 1, 59–67.

1024 Marchant, R., Taylor, D., 1998. Dynamics of montane forest in central Africa during the late
1025   Holocene: a pollen-based record from western Uganda. The Holocene 8, 375–381.
1026   https://doi.org/10.1191/095968398672993971

1027 Marchant, R., Richer, S., Boles, O., Capitani, C., Courtney-Mustaphi, C.J., Lane, P.,
1028   Prendergast, M.E., Stump, D., De Cort, G., Kaplan, J.O., Phelps, L., Kay, A., Olago,
1029   D., Petek, N., Platts, P.J., Punwong, P., Widgren, M., Wynne-Jones, S., Ferro-
1030   Vázquez, C., Benard, J., Boivin, N., Crowther, A., Cuní-Sanchez, A., Deere, N.J.,
1031   Ekblom, A., Farmer, J., Finch, J., Fuller, D., Gaillard-Lemdahl, M.-J., Gillson, L.,
1032   Githumbi, E., Kabora, T., Kariuki, R., Kinyanjui, R., Kyazike, E., Lang, C., Lejju, J.,
1033   Morrison, K.D., Muiruri, V., Mumbi, C., Muthoni, R., Muzuka, A., Ndiema, E.,
1034   Kabonyi Nzabandora, C., Onjala, I., Schrijver, A.P., Rucina, S., Shoemaker, A.,
1035   Thornton-Barnett, S., van der Plas, G., Watson, E.E., Williamson, D., Wright, D.,
1036   2018. Drivers and trajectories of land cover change in East Africa: Human and
1037   environmental interactions from 6000 years ago to present. Earth-Sci. Rev. 178, 322–
1038   378. https://doi.org/10.1016/j.earscirev.2017.12.010

1039 Matthews, J.A., Briffa, K.R., 2005. The 'little Ice Age': Re-evaluation of an evolving concept.
1040   Geogr. Ann. Ser. Phys. Geogr. 87, 17–36. https://doi.org/10.1111/j.0435-
1041   3676.2005.00242.x

1042 Mayewski, P.A., Rohling, E.E., Curt Stager, J., Karlén, W., Maasch, K.A., David Meeker, L.,
1043   Meyerson, E.A., Gasse, F., van Kreveld, S., Holmgren, K., Lee-Thorp, J., Rosqvist,
1044   G., Rack, F., Staubwasser, M., Schneider, R.R., Steig, E.J., 2004. Holocene climate
1045   variability. Quat. Res. 62, 243–255. https://doi.org/10.1016/j.yqres.2004.07.001

1046 Meyers, P.A., 1997. Organic geochemical proxies of paleoceanographic, paleolimnologic, and
1047   paleoclimatic processes. Org. Geochem. 27, 213–250. https://doi.org/10.1016/S0146-
1048   6380(97)00049-1

1049 Miola, A., 2012. Tools for Non-Pollen Palynomorphs (NPPs) analysis: A list of Quaternary
1050   NPP types and reference literature in English language (1972–2011). Rev. Palaeobot.
1051   Palynol., Non-pollen Palynomorphs as Relevant indicators in Palaeoecology and
1052   Archaeobotany 186, 142–161. https://doi.org/10.1016/j.revpalbo.2012.06.010

1053 Morris, P.J., Baird, A.J., Young, D.M., Swindles, G.T., 2015. Untangling climate signals from
1054   autogenic changes in long-term peatland development. Geophys. Res. Lett. 42,
1055   2015GL066824. https://doi.org/10.1002/2015GL066824

1056 Nalepka, D., Walanus, A., 2003. Data processing in pollen analysis. Acta Palaeobot. 43, 125–
1057   134.

1058 Nash, D.J., De Cort, G., Chase, B.M., Verschuren, D., Nicholson, S.E., Shanahan, T.M.,
1059   Asrat, A., Lézine, A.-M., Grab, S.W., 2016. African hydroclimatic variability during
1060   the last 2000 years. Quat. Sci. Rev. 154, 1–22.
1061   https://doi.org/10.1016/j.quascirev.2016.10.012

Nichols, J.E., Peteet, D.M., Moy, C.M., Castañeda, I.S., McGeachy, A., Perez, M., 2014. Impacts of climate and vegetation change on carbon accumulation in a south-central Alaskan peatland assessed with novel organic geochemical techniques. The Holocene 24, 1146–1155. https://doi.org/10.1177/0959683614540729

Nicholson, S.E., Nash, D.J., Chase, B.M., Grab, S.W., Shanahan, T.M., Verschuren, D., Asrat, A., Lézine, A.-M., Umer, M., 2013. Temperature variability over Africa during the last 2000 years. The Holocene 23, 1085–1094. https://doi.org/10.1177/0959683613483618

Nivet, F., Bergonzini, L., Mathé, P.-E., Noret, A., Monvoisin, G., Majule, A., Williamson, D., 2018. Influence of the balance of the Intertropical Front on seasonal variations of rainfall isotopic compositions at Kisiba Masoko (Rungwe Volcanic Province, SW, Tanzania). Isotopes Environ. Health Stud.

Page, S.E., Rieley, J.O., Banks, C.J., 2011. Global and regional importance of the tropical peatland carbon pool. Glob. Change Biol. 17, 798–818. https://doi.org/10.1111/j.1365-2486.2010.02279.x

Peterse, F., Prins, M.A., Beets, C.J., Troelstra, S.R., Zheng, H., Gu, Z., Schouten, S., Damsté, J.S.S., 2011. Decoupled warming and monsoon precipitation in East Asia over the last deglaciation. Earth Planet. Sci. Lett. 301, 256–264. https://doi.org/10.1016/j.epsl.2010.11.010

Powers, L.A., Johnson, T.C., Werne, J.P., Castanada, I.S., Hopmans, E.C., Damste, J.S.S., Schouten, S., 2005. Large temperature variability in the southern African tropics since the Last Glacial Maximum. Geophys. Res. Lett. 32. https://doi.org/10.1029/2004GL022014

Powers, L.A., Johnson, T.C., Werne, J.P., Castañeda, I.S., Hopmans, E.C., Sinninghe Damsté, J.S., Schouten, S., 2011. Organic geochemical records of environmental variability in Lake Malawi during the last 700 years, Part I: The TEX86 temperature record. Palaeogeogr. Palaeoclimatol. Palaeoecol., Southern hemisphere tropical climate over the past 145ka: Results of the Lake Malawi Scientific Drilling Project, East Africa 303, 133–139. https://doi.org/10.1016/j.palaeo.2010.09.006

Riess, K., Bauer, R., Kellner, R., Kemler, M., Piątek, M., Vánky, K., Begerow, D., 2015. Identification of a new order of root-colonising fungi in the Entorrhizomycota: Talbotiomycetales ord. nov. on eudicotyledons. IMA Fungus 6, 129–133. https://doi.org/10.5598/imafungus.2015.06.01.07

Rucina, S.M., Muiruri, V.M., Downton, L., Marchant, R., 2010. Late-Holocene savanna dynamics in the Amboseli Basin, Kenya. The Holocene 20, 667–677. https://doi.org/10.1177/0959683609358910

Russell, J.M., Johnson, T.C., Talbot, M.R., 2003. A 725 yr cycle in the climate of central Africa during the late Holocene. Geology 31, 677–680. https://doi.org/10.1130/G19449.1

Russell, J.M., Johnson, T.C., 2005. A high-resolution geochemical record from Lake Edward, Uganda Congo and the timing and causes of tropical African drought during the late Holocene. Quat. Sci. Rev. 24, 1375–1389. https://doi.org/10.1016/j.quascirev.2004.10.003

Russell, J.M., Johnson, T.C., 2007. Little Ice Age drought in equatorial Africa: Intertropical Convergence Zone migrations and El Niño–Southern Oscillation variability. Geology 35, 21–24. https://doi.org/10.1130/G23125A.1

Russell, J.M., Verschuren, D., Eggermont, H., 2007. Spatial complexity of 'Little Ice Age' climate in East Africa: sedimentary records from two crater lake basins in western Uganda. The Holocene 17, 183–193. https://doi.org/10.1177/0959683607075832

1111   Sachse, D., Radke, J., Gleixner, G., 2004. Hydrogen isotope ratios of recent lacustrine
1112   sedimentary n-alkanes record modern climate variability. Geochim. Cosmochim. Acta
1113   68, 4877–4889. https://doi.org/10.1016/j.gca.2004.06.004
1114   Sauer, P.E., Eglinton, T.I., Hayes, J.M., Schimmelmann, A., Sessions, A.L., 2001.
1115   Compound-specific D/H ratios of lipid biomarkers from sediments as a proxy for
1116   environmental and climatic conditions1. Geochim. Cosmochim. Acta 65, 213–222.
1117   https://doi.org/10.1016/S0016-7037(00)00520-2
1118   Sessions, A.L., Burgoyne, T.W., Schimmelmann, A., Hayes, J.M., 1999. Fractionation of
1119   hydrogen isotopes in lipid biosynthesis. Org. Geochem. 30, 1193–1200.
1120   https://doi.org/10.1016/S0146-6380(99)00094-7
1121   Sinkevičienė, Z., 2016. Caldesia Parnassifolia – not extinct in Lithuania. Bot. Lith. 22.
1122   https://doi.org/10.1515/botlit-2016-0004
1123   Sinninghe Damsté, J.S., Hopmans, E.C., Pancost, R.D., Schouten, S., Geenevasen, J.A.J.,
1124   2000. Newly discovered non-isoprenoid glycerol dialkylglycerol tetraether lipids in
1125   sediments. Chem. Commun. 1683–1684. https://doi.org/10.1039/B004517I
1126   Sinninghe Damsté, J.S., Ossebaar, J., Schouten, S., Verschuren, D., 2012. Distribution of
1127   tetraether lipids in the 25-ka sedimentary record of Lake Challa: extracting reliable
1128   TEX86 and MBT/CBT palaeotemperatures from an equatorial African lake. Quat. Sci.
1129   Rev. 50, 43–54. https://doi.org/10.1016/j.quascirev.2012.07.001
1130   Stockmarr, J., 1971. Tablets with spores used in absolute pollen analysis. Pollen Spores 13,
1131   615–621.
1132   Swan, J.M.A., Gill, A.M., 1970. The origins, spread, and consolidation of a floating bog in
1133   Harvard pond, Petersham, Massachusetts. Ecology 51, 829–840.
1134   https://doi.org/10.2307/1933975
1135   Swindles, G.T., Morris, P.J., Whitney, B., Galloway, J.M., Gałka, M., Gallego-Sala, A.,
1136   Macumber, A.L., Mullan, D., Smith, M.W., Amesbury, M.J., Roland, T.P., Sanei, H.,
1137   Patterson, R.T., Sanderson, N., Parry, L., Charman, D.J., Lopez, O., Valderamma, E.,
1138   Watson, E.J., Ivanovic, R.F., Valdes, P.J., Turner, T.E., Lähteenoja, O., 2018.
1139   Ecosystem state shifts during long-term development of an Amazonian peatland.
1140   Glob. Change Biol. 24, 738–757. https://doi.org/10.1111/gcb.13950
1141   Talling, J.F., Lemoalle, J., ORSTOM, 1998. Ecological dynamics of tropical inland waters,
1142   Cambridge University Press. ed. United Kingdom.
1143   Thevenon, F., Williamson, D., Vincens, A., Taieb, M., Merdaci, O., Decobert, M., Buchet, G.,
1144   2003. A late-Holocene charcoal record from Lake Masoko, SW Tanzania: climatic and
1145   anthropologic implications. The Holocene 13, 785–792.
1146   https://doi.org/10.1191/0959683603hl665rr
1147   Tierney, J.E., Russell, J.M., Huang, Y., Damsté, J.S.S., Hopmans, E.C., Cohen, A.S., 2008.
1148   Northern hemisphere controls on tropical southeast African climate during the past
1149   60,000 Years. Science 322, 252–255. https://doi.org/10.1126/science.1160485
1150   Tierney, J. E., Mayes, M.T., Meyer, N., Johnson, C., Swarzenski, P.W., Cohen, A.S., Russell,
1151   J.M., 2010a. Late-twentieth-century warming in Lake Tanganyika unprecedented
1152   since AD 500. Nat. Geosci. 3, 422–425. https://doi.org/10.1038/ngeo865
1153   Tierney, J. E., Russell, J.M., Eggermont, H., Hopmans, E.C., Verschuren, D., Sinninghe
1154   Damsté, J.S., 2010b. Environmental controls on branched tetraether lipid distributions
1155   in tropical East African lake sediments. Geochim. Cosmochim. Acta 74, 4902–4918.
1156   Tierney, J.E., Lewis, S.C., Cook, B.I., LeGrande, A.N., Schmidt, G.A., 2011. Model, proxy
1157   and isotopic perspectives on the East African Humid Period. Earth Planet. Sci. Lett.
1158   307, 103–112. https://doi.org/10.1016/j.epsl.2011.04.038
1159   Tierney, J.E., Smerdon, J.E., Anchukaitis, K.J., Seager, R., 2013. Multidecadal variability in
1160   East African hydroclimate controlled by the Indian Ocean. Nature 493, 389–392.
1161   https://doi.org/10.1038/nature11785

Trumbore, S., 2009. Radiocarbon and soil carbon dynamics. Annu. Rev. Earth Planet. Sci. 37, 47–66. https://doi.org/10.1146/annurev.earth.36.031207.124300

Tyson, P.D., Lindesay, J.A., 1992. The climate of the last 2000 years in southern Africa. The Holocene 2, 271–278. https://doi.org/10.1177/095968369200200310

van Geel, B., 1978. A palaeoecological study of Holocene peat bog sections in Germany and the Netherlands. Rev. Palaeobot. Palynol. 25, 1–120.

van Geel, B., Gelorini, V., Lyaruu, A., Aptroot, A., Rucina, S., Marchant, R., Damsté, J.S.S., Verschuren, D., 2011. Diversity and ecology of tropical African fungal spores from a 25,000-year palaeoenvironmental record in southeastern Kenya. Rev. Palaeobot. Palynol. 164, 174–190. https://doi.org/10.1016/j.revpalbo.2011.01.002

Vánky, K., 1998. New Australasian Ustilaginales. Mycotaxon 68, 327–344.

Velichkevich, F.Y., Zastawniak, E., 2006. Atlas of the Pleistocene vascular plant macrofossils of Central and Eastern Europe. Part 1-Pteridophytes and monocotyledons. W. Szafer Institute of Botany, Polish Academy of Sciences, Krakow, Poland.

Velichkevich, F.Y., Zastawniak, E., 2009. Atlas of the Pleistocene vascular plant macrofossils of Central and Eastern Europe. Part 2-Herbaceous dicotyledons. W. Szafer Institute of Botany, Polish Academy of Sciences, Krakow, Poland.

Verschuren, D., Laird, K.R., Cumming, B.F., 2000. Rainfall and drought in equatorial east Africa during the past 1,100 years. Nature 403, 410–414. https://doi.org/10.1038/35000179

Verschuren, D., 2003. Lake-based climate reconstruction in Africa: progress and challenges. Hydrobiologia 500, 315–330. https://doi.org/10.1023/A:1024686229778

Verschuren, D., Charman, D.J., 2008. Latitudinal Linkages in Late Holocene Moisture-Balance Variation, in: Battarbee, R.W., Binney, H.A. (Eds.), Natural Climate Variability and Global Warming. Wiley Blackwell, pp. 189–231. https://doi.org/10.1002/9781444300932.ch8

Vincens, A., Williamson, D., Thevenon, F., Taieb, M., Buchet, G., Decobert, M., Thouveny, N., 2003. Pollen-based vegetation changes in southern Tanzania during the last 4200 years: climate change and/or human impact. Palaeogeogr. Palaeoclimatol. Palaeoecol. 198, 321–334. https://doi.org/10.1016/S0031-0182(03)00473-5

Vincens, A., Lézine, A.-M., Buchet, G., Lewden, D., Le Thomas, A., 2007. African pollen database inventory of tree and shrub pollen types. Rev. Palaeobot. Palynol. 145, 135–141. https://doi.org/10.1016/j.revpalbo.2006.09.004

Wanner, H., Solomina, O., Grosjean, M., Ritz, S.P., Jetel, M., 2011. Structure and origin of Holocene cold events. Quat. Sci. Rev. 30, 3109–3123. https://doi.org/10.1016/j.quascirev.2011.07.010

Weijers, J.W.H., Schouten, S., Spaargaren, O.C., Sinninghe Damsté, J.S., 2006. Occurrence and distribution of tetraether membrane lipids in soils: Implications for the use of the TEX86 proxy and the BIT index. Org. Geochem. 37, 1680–1693. https://doi.org/10.1016/j.orggeochem.2006.07.018

Weijers, J.W.H., Schefuß, E., Schouten, S., Damsté, J.S.S., 2007a. Coupled thermal and hydrological evolution of tropical Africa over the Last Deglaciation. Science, New Series 315, 1701–1704.

Weijers, J.W.H., Schouten, S., van den Donker, J.C., Hopmans, E.C., Sinninghe Damsté, J.S., 2007b. Environmental controls on bacterial tetraether membrane lipid distribution in soils. Geochim. Cosmochim. Acta 71, 703–713. https://doi.org/10.1016/j.gca.2006.10.003

Weijers, J.W.H., Panoto, E., van Bleijswijk, J., Schouten, S., Rijpstra, W.I.C., Balk, M., Stams, A.J.M., Damsté, J.S.S., 2009. Constraints on the biological source(s) of the orphan branched tetraether membrane lipids. Geomicrobiol. J. 26, 402–414. https://doi.org/10.1080/01490450902937293

1213 White, F., 1983. Vegetation of Africa - a descriptive memoir to accompany the
1214   Unesco/AETFAT/UNSO vegetation map of Africa.
1215 Woodborne, S., Hall, G., Robertson, I., Patrut, A., Rouault, M., Loader, N.J., Hofmeyr, M.,
1216   2015. A 1000-year carbon isotope rainfall proxy record from south African Baobab
1217   trees (Adansonia digitata L.). PLOS ONE 10, e0124202.
1218   https://doi.org/10.1371/journal.pone.0124202
1219

Highlights

- 4000-year continuous peat record of the Late Holocene in East Africa (SW Tanzania).
- Multi proxy approach evidences major ecological changes at ca. 2500 yr cal. BP.
- Detailed temperature and hydrology records highlight several cold events.
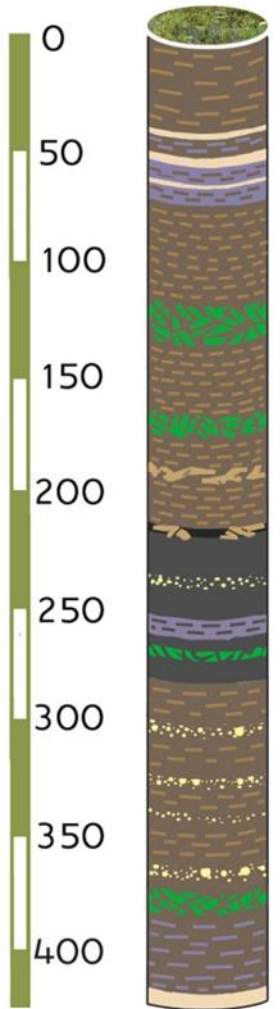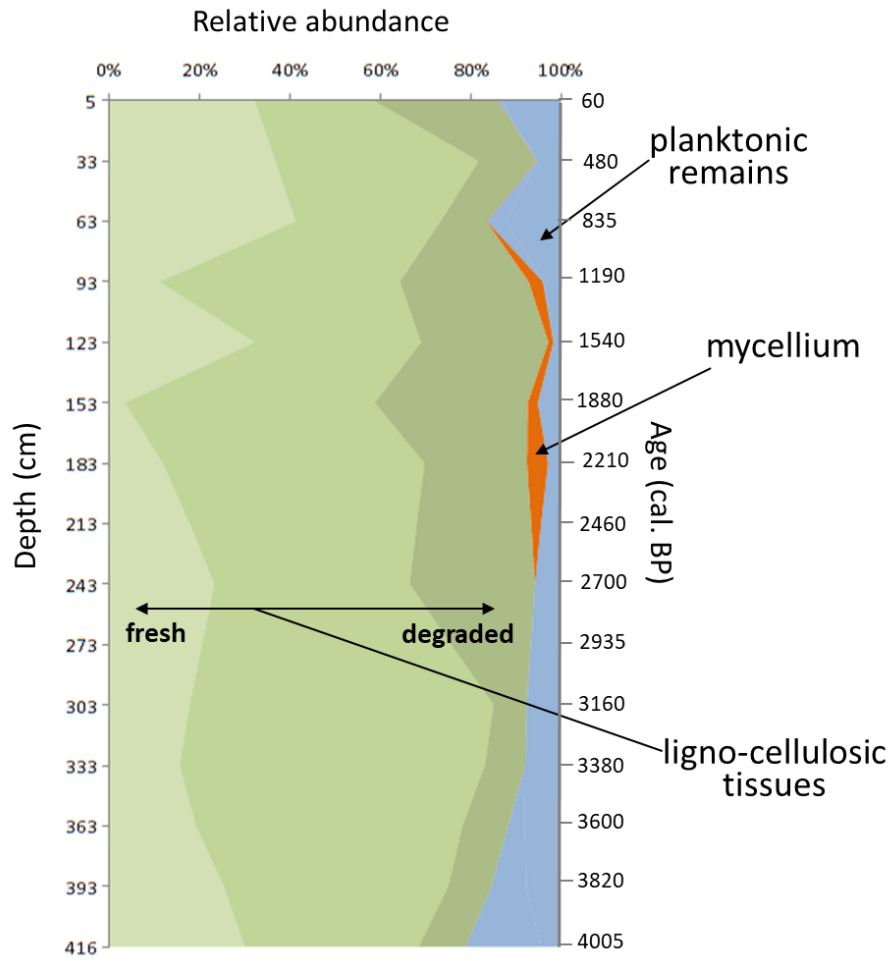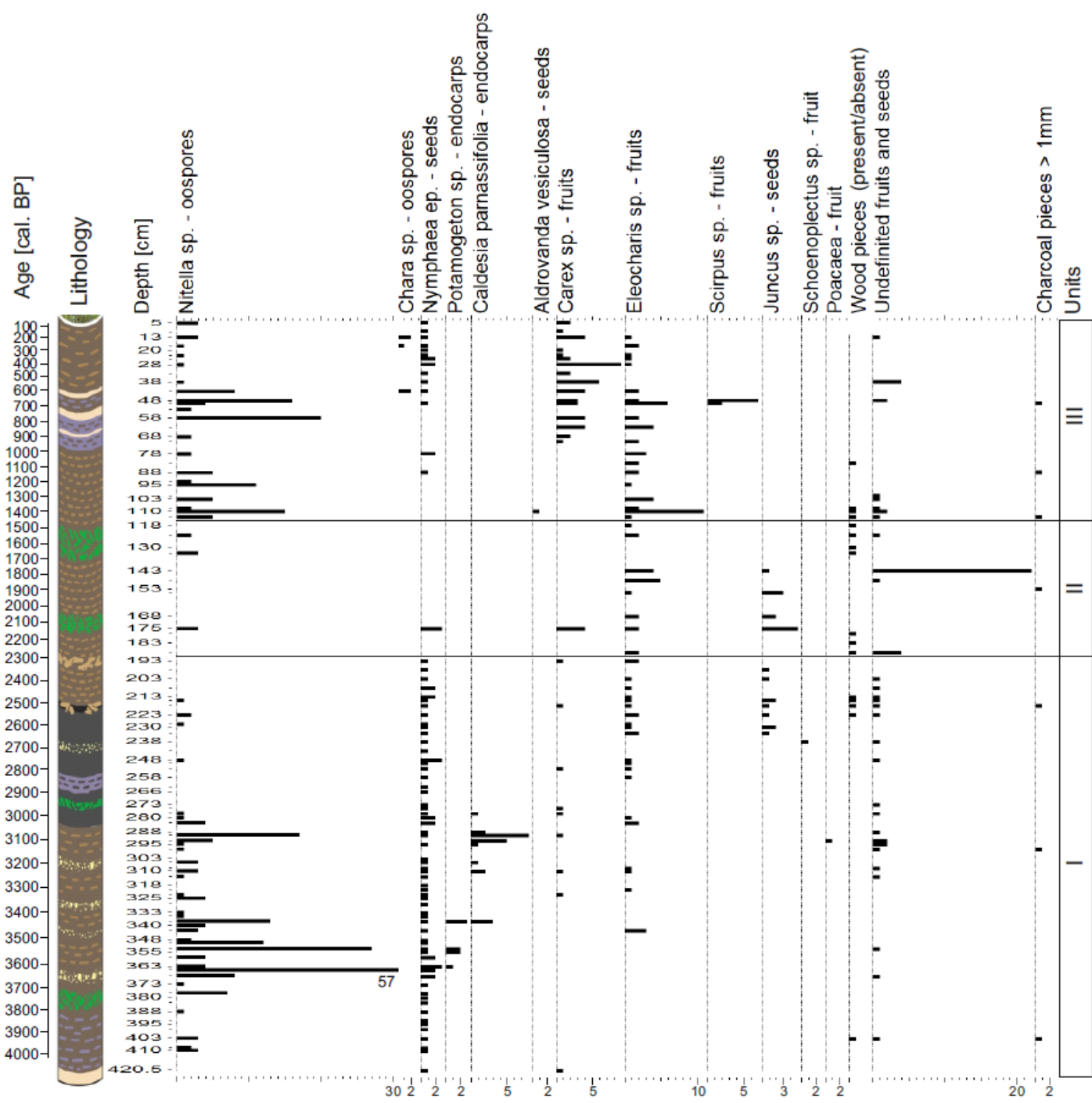- More recent climate conditions seem connected to South African climate variability.
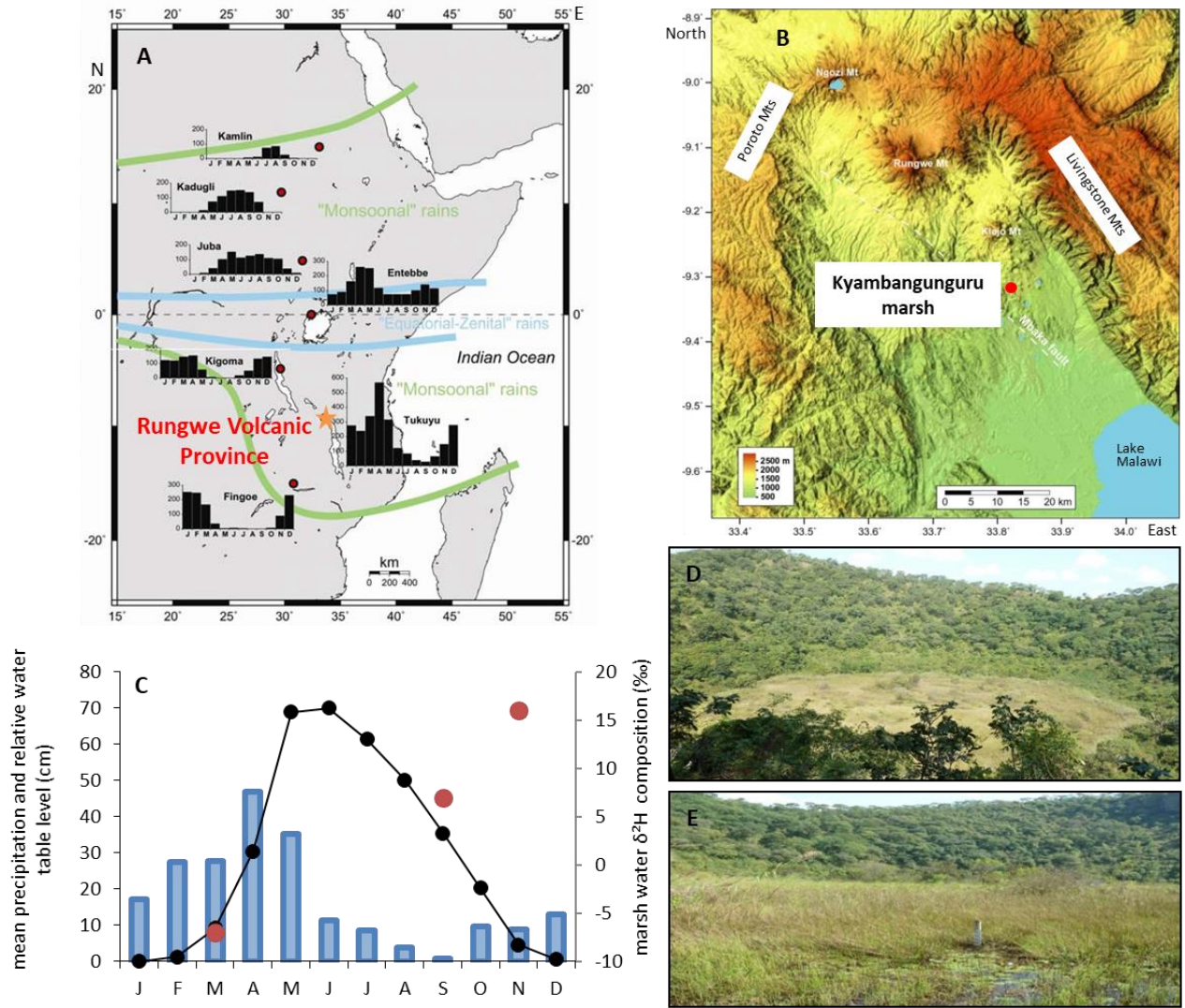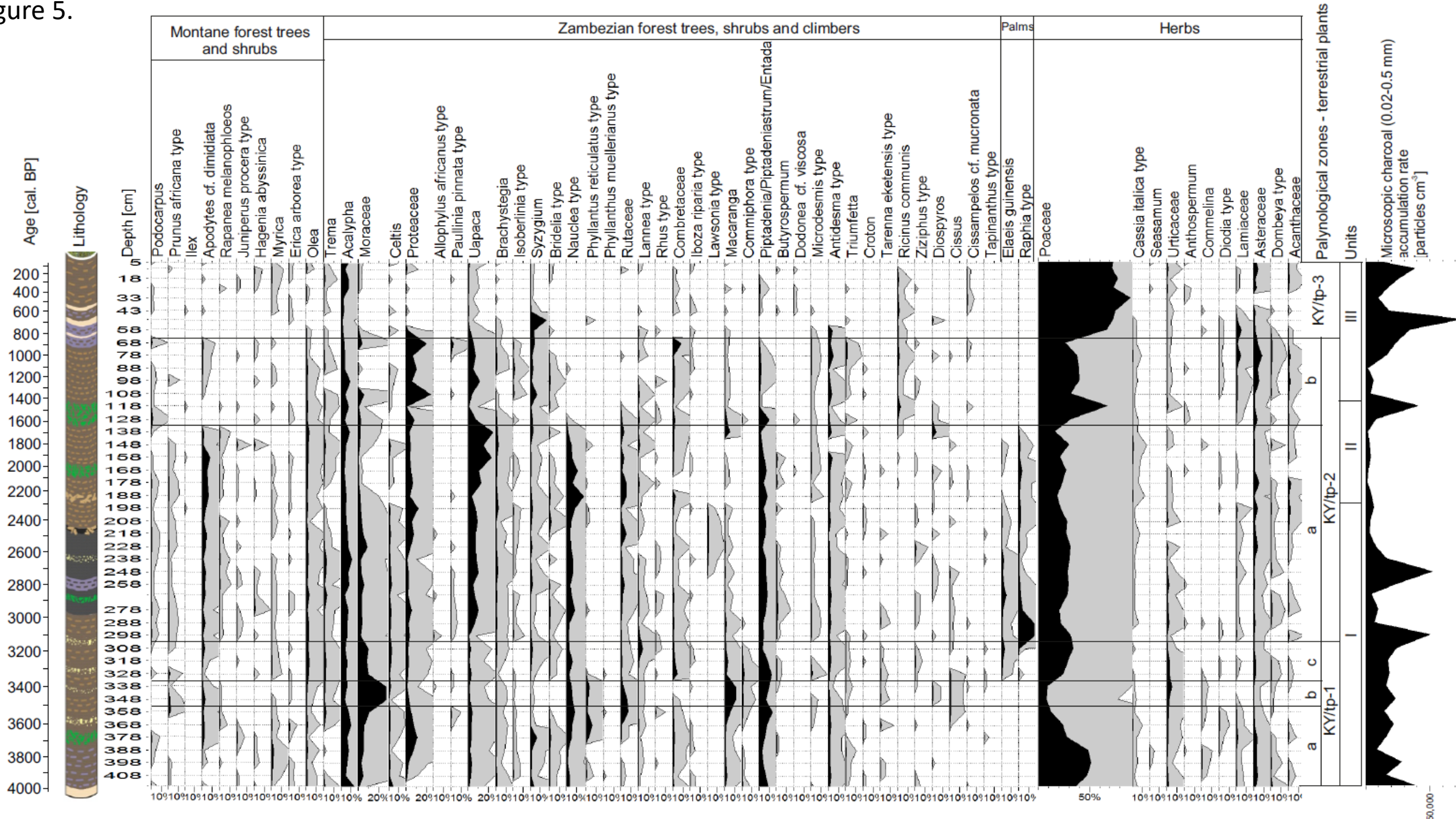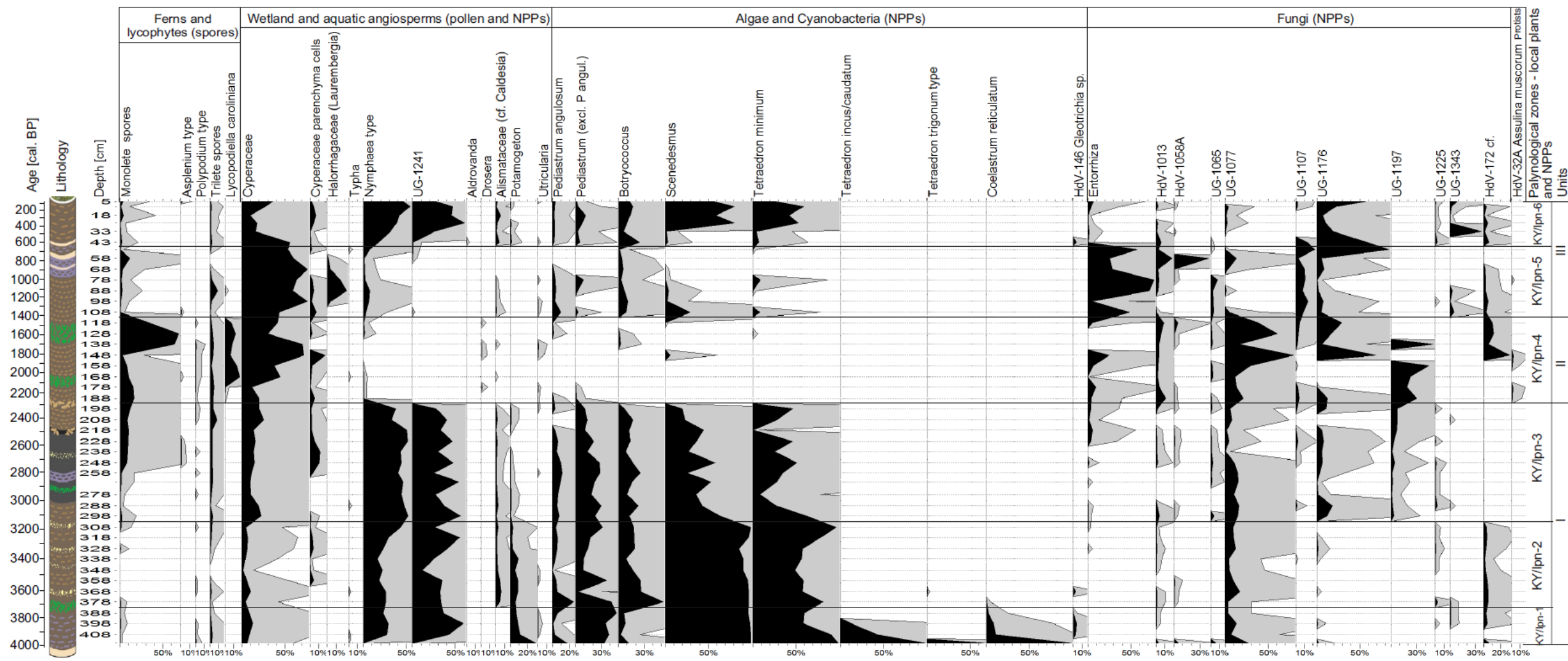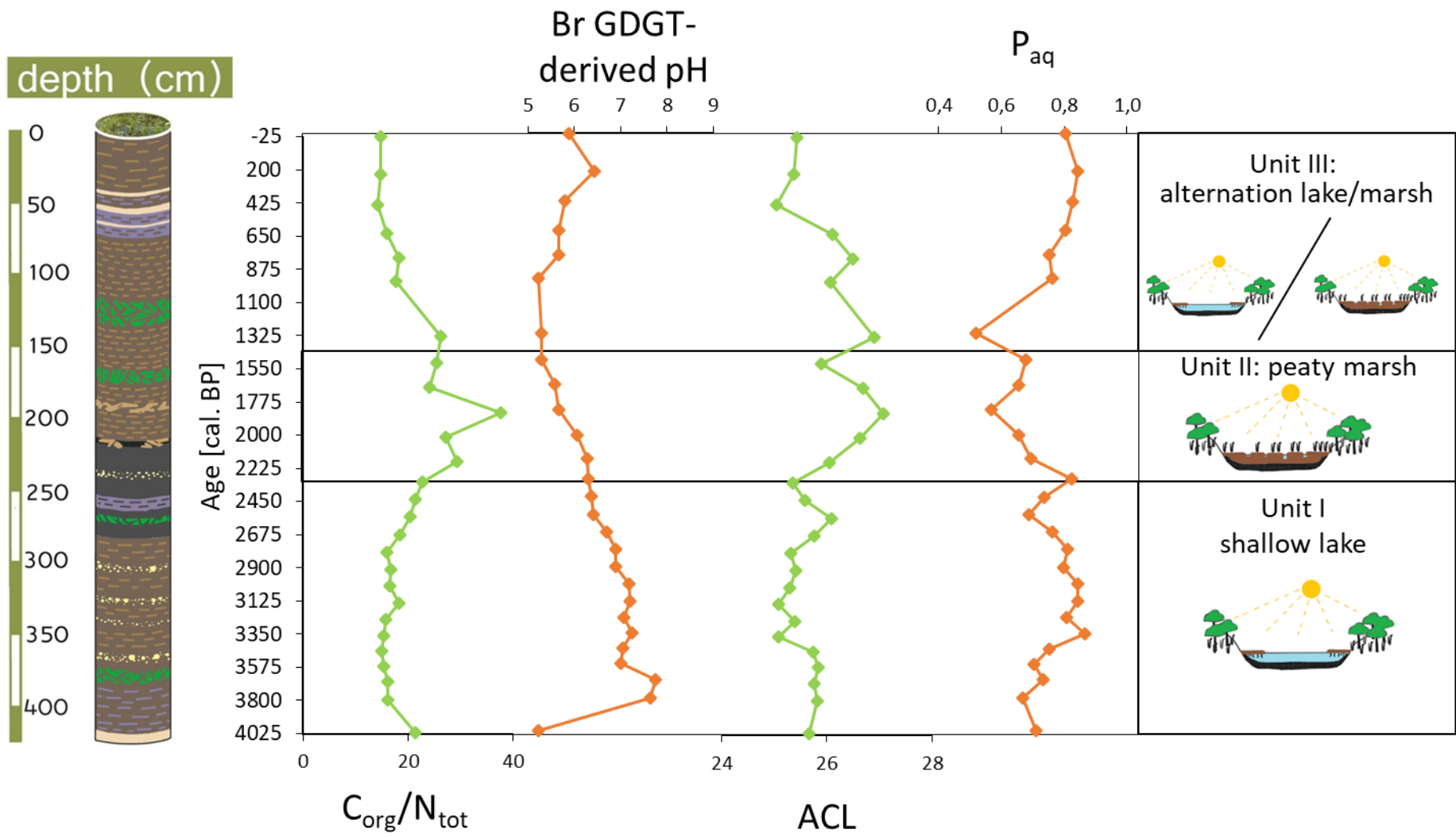
Figure 1.
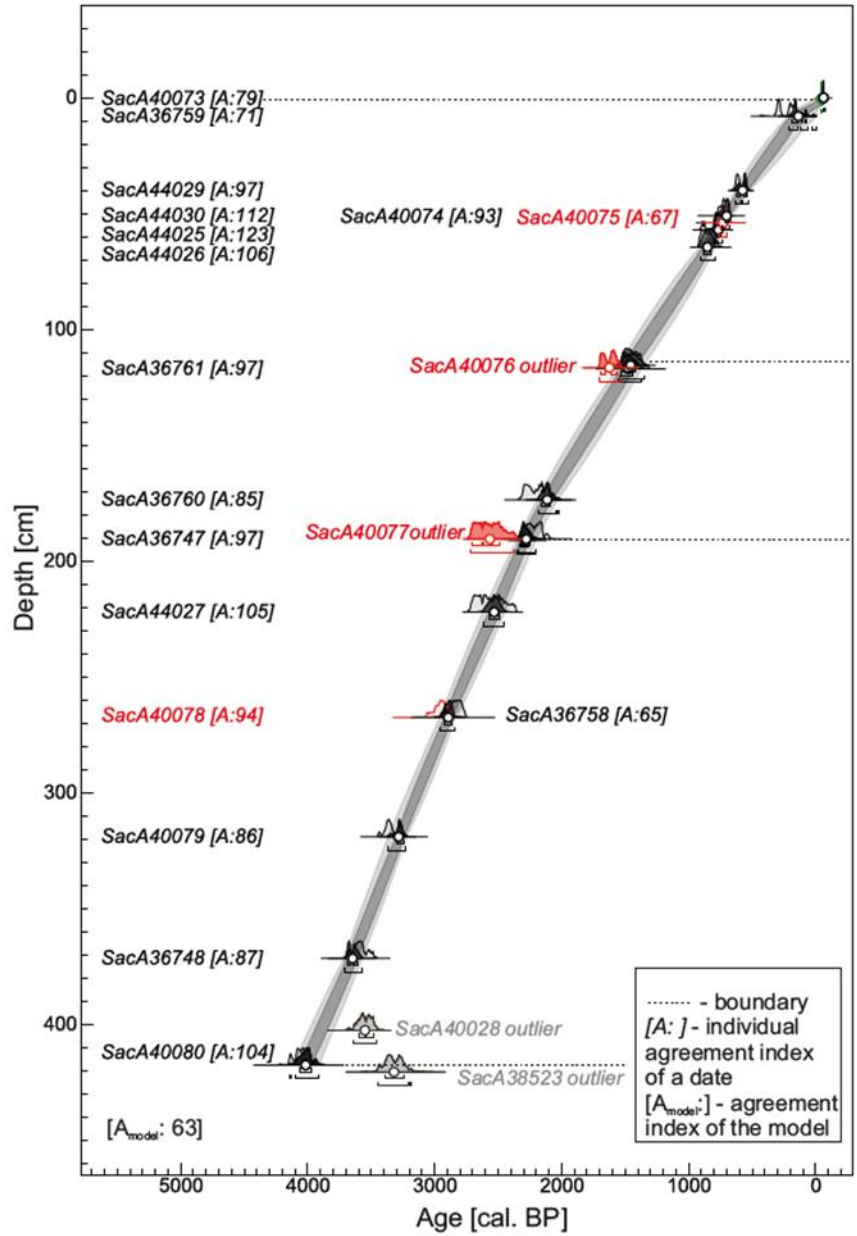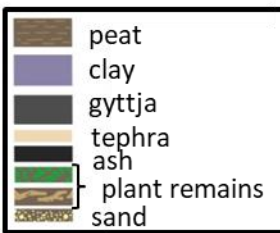
Figure 2.

Figure 3.

Figure 4.

Figure 5.

Figure 6.

Figure 7.
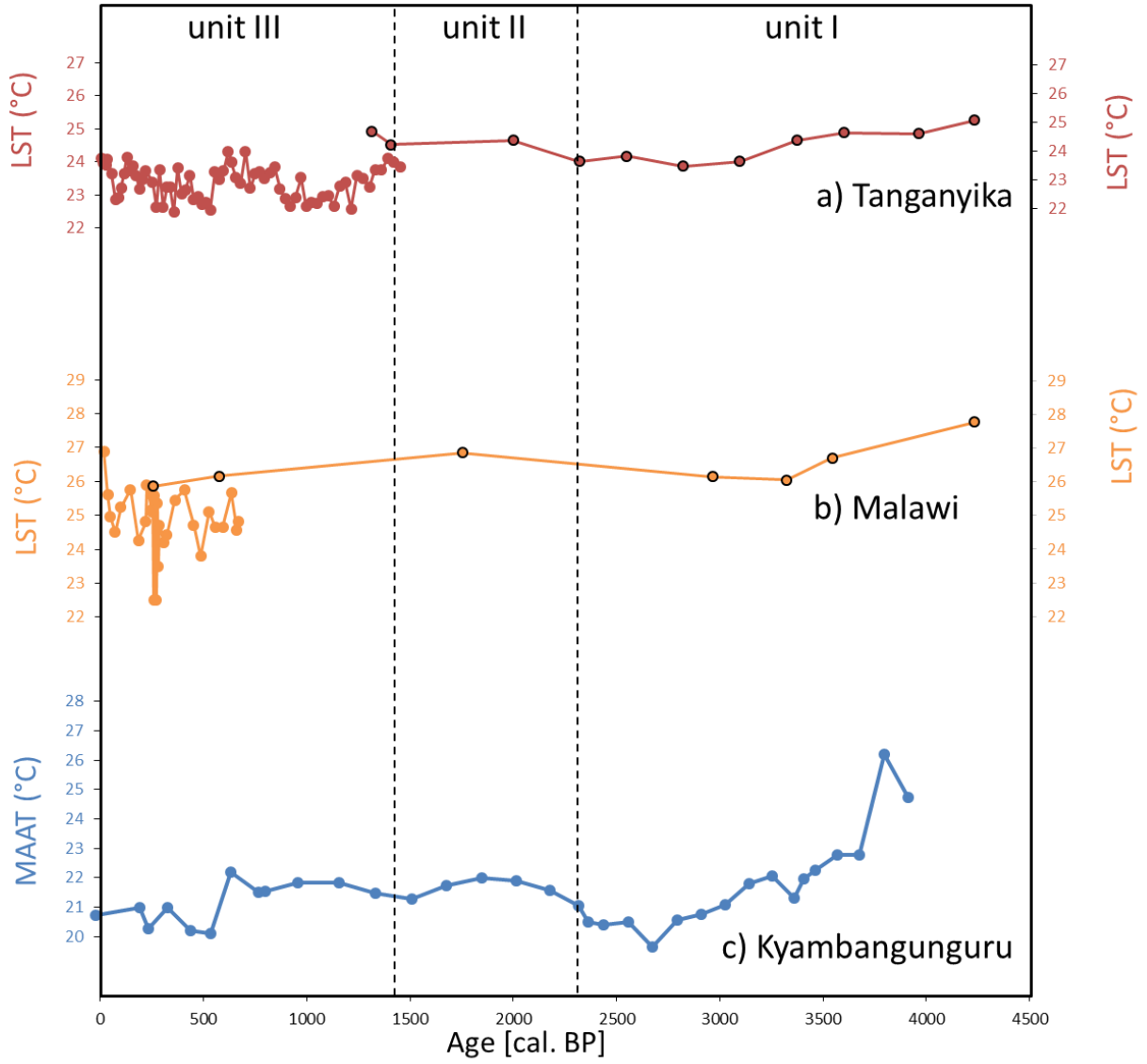
Figure 8.
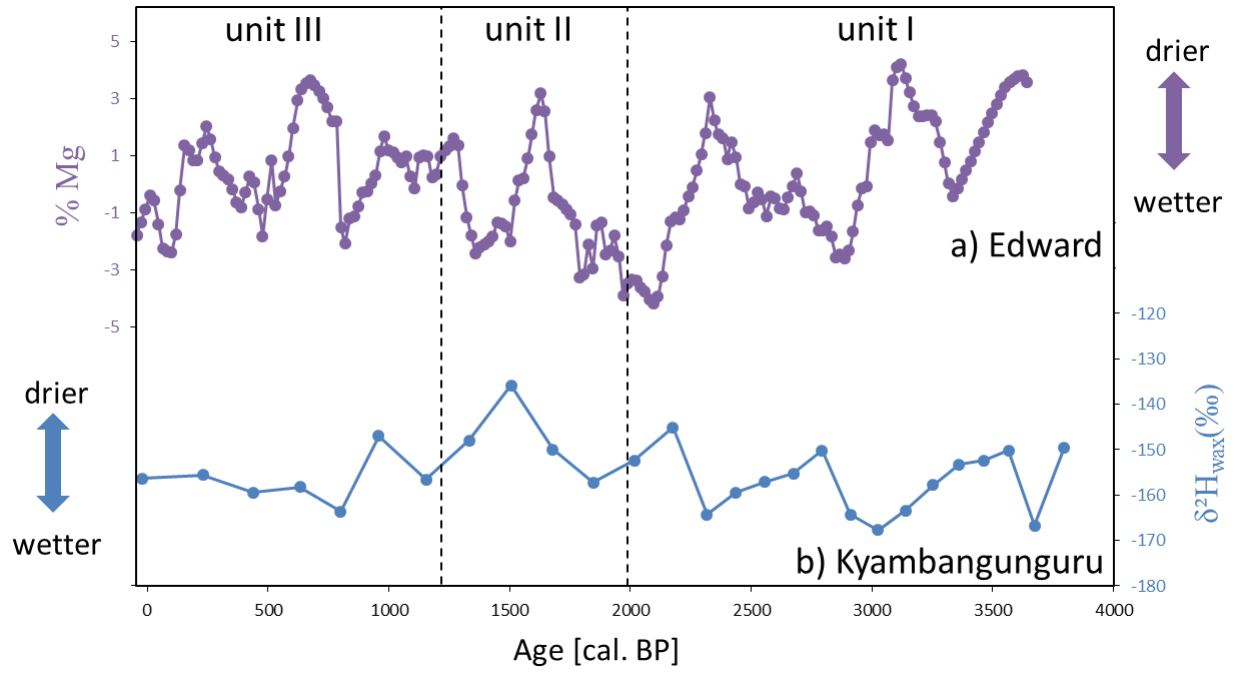
Figure 9.

Table 1.

Depth (cm)	AMS ^{14}C measure ref	Type of material	Carbon mass (mg)	^{14}C activity (pMC)	Measured ^{14}C age (cal. BP)	Calibrated age range [cal. BP; 95.4% (2 σ) range]	Modelled age ± σ error (cal. BP)	δ^{13}C (‰)
0.5	SacA40073	TOM	1.82	112.21 ± 0.33	Post 1950	-8–-8 (3.3 %) -43–-46 (88.4 %) -47–-47 (3.7 %)	-45±5	-29.5
8.0	SacA36759	TOM	0.75	96.86 ± 0.43	255 ± 35	435–408 (1.9 %) 325–254 (39.4 %) 225–143 (54.2 %)	135±50	-24.5
40.0	SacA44029	TOM	0.75	92.48 ± 0.24	630 ± 30	646–588 (58.7 %) 574–535 (36.7 %)	574±28	-23.8
51.0	SacA44030	TOM	0.75	89.99 ± 0.27	845 ± 30	763–673	701±15	-22.9
54.0	SacA40074	TOM	0.55	89.53 ± 0.29	890 ± 30	800–682	730±14	-28.0
54.0	SacA40075	Wood	0.91	90.27 ± 0.36	825 ± 30	742–666	729±14	-25.2
57.0	SacA44025	TOM	0.75	89.20 ± 0.23	920 ± 30	905–861 (14.1 %) 842–829 (1.3 %) 820–724 (80 %)	765±17	-21.4
64.0	SacA44026	TOM	0.75	88.55 ± 0.24	975 ± 30	921–774	852±30	-20.2
116.5	SacA36761	TOM	0.50	82.03 ± 0.48	1590 ± 45	1538–1348 (94.6 %) 1331–1324 (0.8 %)	1472±47	-25.5
116.5	SacA40076	Wood	1.37	80.47 ± 0.28	1745 ± 30	1702–1639 (39.3 %) 1633–1542 (56.1 %)	Not applied	-28.2
173.5	SacA36760	TOM	0.75	75.90 ± 0.38	2215 ± 40	2318–2059	2113±37	-20.1
190.5	SacA36747	TOM	0.75	75.68 ± 0.31	2240 ± 35	2328–2146 (90.1 %) 2131–2103 (5.3 %)	2278±34	-25.0
190.5	SacA40077	Wood	1.30	73.12 ± 0.26	2515 ± 30	2719–2379	Not applied	-27.5
222.0	SacA44027	TOM	0.75	73.18 ± 0.22	2510 ± 30	2715–2379	2531±42	-26.8
267.5	SacA36758	TOM	0.75	70.72 ± 0.37	2785 ± 40	2945–2759	2892±30	-27.9

267.5	SacA40078	Wood	1.40	69.87 ± 0.25	2880 ± 30	3062–2857	2893±30	-27.9
319.0	SacA40079	TOM	1.11	67.41 ± 0.25	3170 ± 30	3445–3423 (4.8%) 3411–3236 (90.6 %)	3283±34	-28.6
371.5	SacA36748	TOM	0.75	65.50 ± 0.29	3395 ± 35	3692–3657 (10.4 %) 3651–3478 (85 %)	3646±37	-28.2
402.0	SacA44028	TOM	0.75	65.76 ± 0.21	3365 ± 30	3639–3456	Not applied	-26.4
417.5	SacA40080	TOM Tephra	1.04	62.75 ± 0.24	3745 ± 30	4151–3960 (91.1 %) 3950–3926 (4.3 %)	4015±47	-20.0
420.5	SacA38523	TOM Tephra	0.30	67.47 ± 0.42	3160 ± 50	3450–3206 (93.8 %) 3197–3182 (1.6 %)	Not applied	-23.6